EUROPEAN COMMISSION

Community Research

NF-PRO

Contract Number: FI6W-CT-2003-02389

DELIVERABLE (D-N°:2.5.10)

Author(s): A. Meleshyn, T. Reeck, M. Azeroual, C. Bunnenberg, B. Riebe, G. Houben

Reporting period: e.g. **2004-2006**

Date of issue of this report: **2006/09/30**
Version : **final report**

NF-PRO RTD Component: 1
NF-PRO Work Package : WP 2.5

Start date of project : **01/01/2004** Duration : 48 Months

	Name	Date	Signature for approval
Author[1]:			
Verified by[2]:			
Approved by[3]:			
Verified by RTD Leader			

[1] Name and signature of the person responsible for drafting the deliverable
[2] Name and signature of the reviewer (member of applicable Work Package)
[3] Name and signature of the Work Package Leader
[4] Name of the RTDC Leader. The RTDC Leader is informed on the availability of the deliverable and verifies whether the introduction, formulation of objectives, interfaces to other project activities and conclusions are sufficiently clear to allow integration of the deliverable into the overall work programme of NF-PRO.

Project co-funded by the European Commission under the Euratom Research and Training Programme on Nuclear Energy within the Sixth Framework Programme (2002-2006)		
Dissemination Level		
PU	Public	
RE	Restricted to a group specified by the partners of the [NF-Pro] project	
CO	Confidential, only for partners of the [NF-Pro] project	

DISTRIBUTION LIST

Name	Number of copies	Comments
Michel RAYNAL (Project Officer European Commission)	2	
Luc van Loon (Work package Leader)	1	
(RTDC Leader)	1	
Alain SNEYERS Coordinator NF-PRO		

Reactive transport of uncharged radionuclide complexes through clay membranes

This project is performed with the European Commission in the sixth framework of its programme on Management of Radioactive Waste:

Understanding and Physical and Numerical Modelling of the Key Processes in the Near-Field and their Coupling for Different Host Rocks and Repository Strategies (NF-PRO)

September 2006

Reactive transport of uncharged radionuclide complexes through clay membranes

Summary

The interaction of the $Ca_2UO_2(CO_3)_3$ complex (CaUC complex) with Na- and Ca-exchanged MX-80 bentonite was investigated in batch and diffusion experiments.

The uncharged CaUC complex was successfully synthesized and found to remain stable in solution. Detection and relative quantification of charged and uncharged uranyl species were performed using Laser-Induced Fluorescence spectroscopy (LIF). For the non-destructive uranium detection in solid samples the Micro-Roentgen-Fluorescence Analysis (µ-RFA) was applied, while multi-element analyses were carried out by Inductively Coupled Plasma Atom Emission Spectrometry (ICP-AES) and Inductively Coupled Plasma Mass Spectrometry (ICP-MS).

Batch experiments show that the CaUC complex is relatively stable when exposed to a Ca-bentonite suspension. Na-MX-80 suspensions, however, are able to destabilize up to 40 % of the initial amount through uranyl uptake from the complex and parallel Na release. The immediate consequence is that Na-bentonite should be preferred instead of Ca-bentonite when applied in a geotechnical barrier system.

In diffusion cell experiments with Ca-bentonite compacted to a dry density of 1.6 $g \cdot cm^{-3}$, migration of the U(VI) front was only about 0.5 mm in 196 days. However, trace amounts of U(VI) arrived at the lower end of the 5-mm pellet after this time leading to an outlet uranium concentration of 0.25 % of that in the inlet solution.

1 Aim and scope of this study

The activities envisaged in this work aimed at the clarification of the interaction of uncharged radionuclide complexes with clays. While considerable attention has been paid to sorption mechanisms of natural and modified clays to retain cationic and anionic radionuclides, very little is known on the migration behaviour of uncharged aqueous complexes within a clay barrier.

As clays often contain carbonates, the pH of the pore water of clay material in a waste repository for nuclear waste is expected to be in the range of 6.5 – 9.0. In this pH-range, formation of sulphate and carbonate complexes is likely to occur.

For experiments on the interaction of such complexes with MX-80 bentonite, the uncharged calcium uranyl carbonato complex $Ca_2UO_2(CO_3)_3$ was selected. At pH 7.0 to 9.5 this complex is present with a probability of 95 % in the Ca^{2+} - UO_2^{2+} - CO_3^{2-} - system. Since the aquatic calcium uranyl carbonato complex (CaUC) shows a characteristic fluorescence pattern after laser excitation in the UV range (266 and 337 nm), the migration of this compound and the composition of the species can be followed by evaluating laser-induced fluorescence spectra.

2 Survey of literature on uncharged radionuclide complexes

Aqueous radionuclide transport can be considered as the main pathway of radionuclide migration from the disposal site into the biosphere. This identifies the water solubility of a neutral radionuclide complex as a condition for its relevance. Another important criterion for an assessment of the transport ability of a neutral radionuclide complex is the value of its stability constant $\log\beta$. Large stability constants indicate that such a complex does not dissociate readily in response to changes of the chemical environment on its migration path.

Available experimental data indicate that the following aqueous neutral complexes conform to these two criteria and, hence, a special attention should be paid to these compounds while carrying out the safety analysis of a geological repository for radioactive wastes:

$UO_2(IO_3)_2$	$\log\beta = 3.05 \pm 0.10$	[Karbowiak *et al.* 1996],
UO_2SO_4	$\log\beta = 3.35 \pm 0.15$	[Geipel *et al.* 1996],
$Nd(C_2H_3O_2)_3$	$\log\beta = 3.58 \pm 0.08$ (T=25°C),	
	$\log\beta = 4.71 \pm 0.10$ (T=70°C)	[Zanonato *et al.* 2001],
$UO_2(C_2H_3O_2)_2$	($\log\beta = 4.37 \pm 0.14$ (T=25°C),	
	$\log\beta = 5.27 \pm 0.09$ (T=70°C)	[Jiang *et al.* 2002],
$UO_2C_4H_4O_5$	$\log\beta = 5.01 \pm 0.04$ (T=25°C),	
	$\log\beta = 5.38 \pm 0.10$ (T=70°C)	[Rao *et al.* 2003],
PuO_2CO_3	$\log\beta = 8.7 \pm 0.3$	[Pashalidis *et al.* 1997],
UO_2CO_3	$\log\beta = 8.93 \pm 0.05$	[Pashalidis *et al.* 1997],
NpO_2CO_3	$\log\beta = 9.02 \pm 0.10$	[Kato *et al.* 1998],
$Th(C_2H_3O_2)_4$	$\log\beta = 10.25 \pm 0.19$ (T=25°C),	
	$\log\beta = 11.54 \pm 0.20$ (T=70°C)	[Rao *et al.* 2004],
UO_2HPO_4	$\log\beta = 19.87 \pm 0.29$	[Brendler *et al.* 1996],
$Ca_2UO_2(CO_3)_3$	$\log\beta = 30.55 \pm 0.25$	[Bernhard *et al.* 2001],
$UO_2(H_2PO_4)_2$	$\log\beta = 46.09 \pm 0.22$	[Brendler *et al.* 1996]

Although the $UO_2(H_2PO_4)_2$ complex has the highest stability constant, it is commonly formed only in solutions having PO_4^{3-}/CO_3^{2-} ratios greater than 10 [Bostick *et al.* 2002], which is rather untypical of the expected chemical composition of the solution at the disposal site. The situation is, however, very different for the second most stable complex, $Ca_2UO_2(CO_3)_3$. Calcium is present in the materials utilized in the repository design, and dissolved CO_2 will be available there as a ubiquitous component of the groundwater as soon as the latter enters the disposal site. Based on the above

data, it can therefore be expected that the formation of the calcium uranyl carbonato complex $Ca_2UO_2(CO_3)_3$ could become a critical mechanism of uranium transport through the clay barrier into the geological environment and hence into the biosphere. Indeed, the sorption of aqueous UO_2^+ onto ferrihydrite and soil clay components decreases by more than an order of magnitude due to the formation of this neutral complex [Zheng *et al.* 2003].

Sorption of uranyl onto Na-montmorillonite, the latter being the main component of the proposed engineered bentonite barrier, decreases considerably (by about 70%) at the addition of small amounts of calcite (about 1.5 weight%) and subsequent formation of the calcium uranyl carbonato complex [Kowal-Fouchard *et al.* 2004]. Another effect, which can result in an increasing rate of uranium migration through engineered barriers and the host rock as well as in an increasing bioavailability in the biosphere, is that the formation of $Ca_2UO_2(CO_3)_3$ complex strongly inhibits the bacterial reduction of the U(VI) form to the much less soluble U(IV) form [Brooks *et al.* 2003].

3 *Experimental set-up and performance*

3.1 Synthesis of the CaUC-complex

The synthesis of the CaUC-complex solution was performed by adopting the instructions for the synthesis of liebigite ($Ca_2[UO_2(CO_3)_3] \cdot 10\ H_2O$) as described by Amayri (2002). The required components, $UO_2(NO_3)_2 \cdot 6\ H_2O$, Na_2CO_3 and $Ca(NO_3)_2 \cdot 4\ H_2O$, were combined at a ratio of 1:3:2 and diluted 1/25 compared to the original recipe to prevent the CaUC-complex from crystallisation. On the basis of experimental information obtained from EXAFS measurements [Bernhard *et al.,* 2001] the complex can be visualized as shown in Fig. 3.1

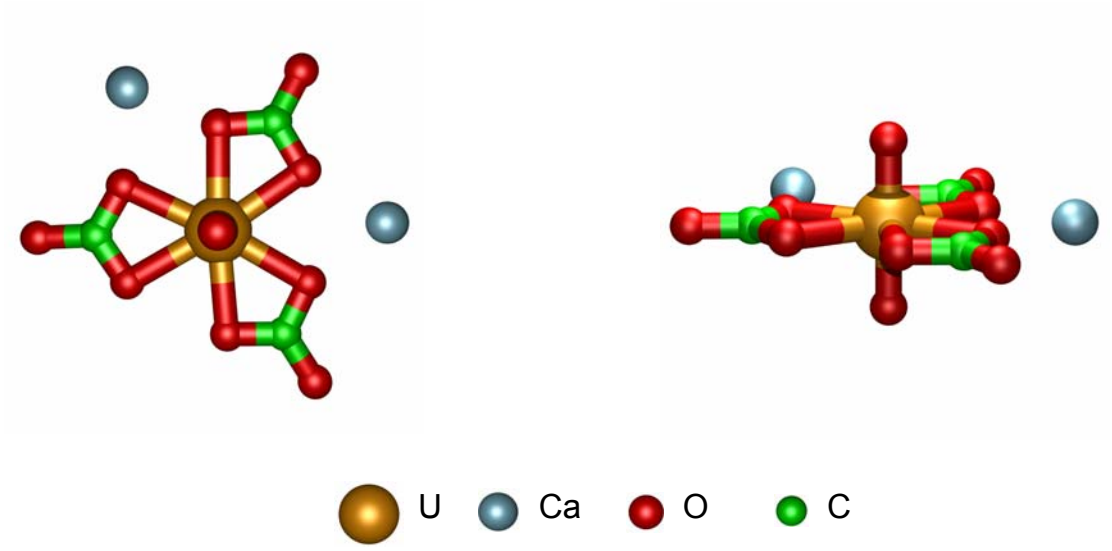

Fig. 3.1: $Ca_2UO_2(CO_3)_3$ complex: Top (left) and side view (right) with respect to its equatorial plane.

The pH-value of the solution following synthesis was 8.1 to 8.2. Under the influence of the laboratory atmosphere, however, it decreased to pH 7.4 to 7.5 after 3 weeks. This is still well within the stability range of the CaUC-complex.

3.2 Laser-induced fluorescence spectroscopy (LIF)

The specific luminescence behaviour of compounds containing uranium(IV) or uranium(VI) following optical stimulation is widely used for qualitative and quantitative analyses. Especially laser-induced spectrofluorometry is one of the most sensitive techniques for the determination of uranium at trace levels. Moreover, as different

uranyl complexes show individual spectral signatures and due to the linearity of the process over a sufficiently broad range of concentrations, application of this spectroscopic method allows fast and direct detection of the speciation of the sample.

The experimental set-up applied was elaborately tested and optimized during preliminary experiments and proved to be well suited to fulfil the requirements and constraints of the given task.

In the majority of measurements a nitrogen laser operating at 337 nm and delivering about 400 µJ of energy in 500 ps pulses with a repetition rate of 10 Hz was used as the excitation source. The beam was coupled in a UV-grade optical fibre and guided to a 4 ml quartz cell. The subsequently emitted fluorescence is collected at right angles to the excitation beam by a second fibre and is dispersed by a monochromator (MS125, 300 l/mm, LOT Oriel). The wavelength-dependent fluorescence intensity is measured by a peltier-cooled CCD-camera (EEV CCD40-11, 1024x128, InstaSpecIV, AndorTechnology). The spectra were digitized by a 16-bit AD-card under software-control, which additionally allowed simple pre-processing of the data.

For each single spectrum, at least 1,200 laser pulses were accumulated, in order to improve the signal/noise ratio and to keep the measuring time within acceptable limits. For further processing of the raw spectral data, in-house developed software was used. Besides the normalisation routines, a deconvolution of the fluorescence emission is most important. The detected emission corresponds approximately to a linear superposition of all individual fluorescent compounds involved, including perturbations (e.g. reabsorption, quenching or inner filter effects). Hence, spectral deconvolution involves solving a least-squares problem for a linear equation with nonnegative constraints. The required coefficients for a set of appropriate base-spectra were calculated using singular value decomposition by implementing a MATLAB-based routine. The software allows monitoring of the fitting process and enables to easily test several hypotheses according to the speciation calculations. By this it is possible to generate a suitable matrix of base-spectra depending on the current chemical constraints (pH, etc.) and to apply the well-known principle of parsimony or “Occam's Razor“, wherever ambiguous situations appear. Extensively discussed in the literature (e.g. by Meinrath, 1998) it is, above all, a practical way to diminish the risk of overfitting and wrong deductions (see Fig. 3.2).

As an additional laser-system, a Nd-YAG laser (NL 303G, Ekspla, Lithuania) and an intensified CCD-camera (iStar, AndorTechnology) was used. After the laser beam has passed a fourth-harmonic-generator (FHG), the system allowed an alternative sample excitation at a wavelength of 266 nm. Operating with a repetition rate of 10 Hz the laser provided 7 ns pulses of an adjustable energy up to 20 mJ. For dispersion of the emitted fluorescence, the same type of monochromator was used

(MS125, see above). The peltier-cooled ICCD-camera (E2V-30-11, eff. 690x256, 16 bit) and the integrated digital delay generator was used to record time-resolved fluorescence decays of the samples. All functions, like variable delay time, gate width, and signal amplification, were fully under software control.

In the limited time of access, this second system was used for verification purposes of the experimental results. The additional excitation wavelength in the UV has proven to be useful in several crucial situations, and it is of vital importance during the interpretation of recorded spectra. Especially a different sensitivity to humic substances and the separation of emitting species due to their individual fluorescence decay times could be utilized in the experiments. Furthermore, the lower limit of detection of the second laser-system allowed the confirmation and cross-validation of executed concentration measurements.

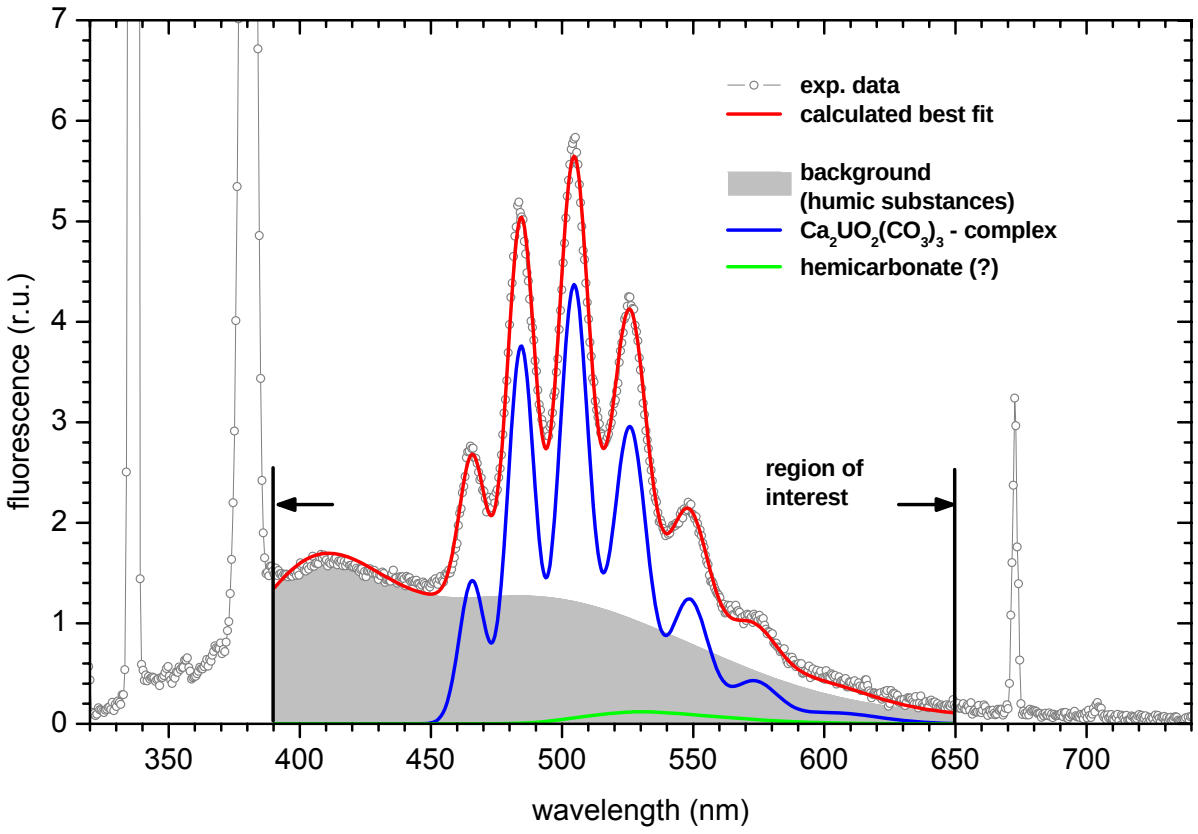

Fig. 3.2: Principal shapes and components of LIF spectra of the CaUC complex in a Ca-bentonite suspension (filtered before measurement). Red, green and blue coloured lines represent the specific content of the indicated fluorescent uranyl-species.

3.3 Micro X-ray fluorescence (micro-XRF)

The analytical principle of the X-ray fluorescence (XRF) is based on the excitation of atoms by X-rays and the subsequent emission of fluorescence radiation, which is characteristic for the emitting atom. This X-radiation is detected by a Si-semiconductor detector, where the concentration of the element in question can be deduced from the fluorescence intensity. In the determination of the uranium distribution within the clay pellets of the diffusion cells, an micro X-ray fluorescence instrument (Eagle µProbe, RÖNTGENANALYTIK MESSTECHNIK GmbH) was applied. Focusing optics reduced the measuring area to a spot of 50 µm, which allowed a correspondingly high spatial resolution in the surface scan.

In all measurements the X-ray device was set to a voltage of 40 kV, a current of 1000 µA and a time constant of 6 µs. The detection limit for the uranium concentrations was 0.0001 mmol/g. In the course of this study, micro-XRF was applied to determine uranium distributions in vertical sections of the diffusion pellets either as a scan of the total cross section (see Figs. 4.11 and 4.13) or as a vertical line scan to demonstrate the progress of the diffusion front (see Figs. 4.12 and 4.14).

3.4 Inductively Coupled Plasma – Atomic Emission Spectrometry (ICP-AES) and – Mass Spectrometry (ICP-MS)

Both spectrometers were developed for the analysis of trace amounts of elements in solution, where the detection limit of ICP-MS is about three orders of magnitude lower than that of ICP-AES. In both systems the excitation source is an inductively coupled argon plasma operating at a temperature of 5.000 to 7.000 K.

In the case of an AES spectrometer (sometimes also referred to as Optical Emission Spectrometer, OES), the induced light emission of the excited atoms is splitted into element-specific wavelengths and detected by a series of photomultiplier tubes. Light intensities are proportional to the abundance of the element in question. Advantages of this analytical method include simultaneous detection of up to 60 elements, broad range of linear calibration and low matrix effects.

ICP-AES analyses were performed at the Institute of Inorganic Chemistry (Leibniz University Hannover) with a Spectroflame Modula ICP-OES instrument. Detection limits of some relevant elements are given in Table 3.1. The method was applied to investigate the association of uranium species with colloid fractions after contact with Na- and Ca-bentonites (Fig. 3.3).

Table 3.1: ICP-AES detection limits

Element	Si	U	Na	Mg	Al	Ca	Fe
[ppm]	0.02	0.03	0.02	0.005	0.02	0.02	0.03
[µmol/L]	0.8	0.1	0.8	0.2	0.6	0.5	0.5

For the MS analysis, the positively charged ions pass two apertures (sampler and skimmer) and an electrostatic lens system to arrive in the high-vacuum vessel of the quadrupole-mass-spectrometer. In this vessel, the ions are separated according to their mass-to-charge ratio and detected by means of a charge-sensitive detector. The advantages of this method are small samples, low detection limits as well as fast and simultaneous measurements of a great number of elements from lithium-6 up to uranium-238. ICP-MS analyses were performed with an ELEMENT1/Thermo instrument at the BGR.

3.5 Cation exchange capacity of the clay material

All research teams used sub-portions of the same clay material (Volclay, provided by Südchemie AG), to guarantee comparability of the results.

The CEC (cation exchange capacity) was determined at the BGR laboratory by the Cu-triene method (slightly modified after Kahr & Meier (1996)). The Cu-triene solution is produced by adding 1.596 g $CuSO_4$ (dried) to 100 ml water, then adding 1.463 g triethylene-tetramine (triene), and finally adding water up to 1000.0 ml. The samples were dried at 60 °C maximum. The water content was determined by drying 1 g at 105 °C for 2-3 days. For the determination of the CEC, 0.1000 g and 0.1500 g were weighed in 85 ml centrifuge tubes. Finally, 10.0 ml of the 0.01 M Cu-triene solution and 50.0 ml water were added. Before centrifugation the suspension was kept for 2 h in an end-over-end shaker. The supernatant was analyzed with respect to vis-absorption at 578 nm against water. In addition the vis-absorption of the pure Cu-triene solution (diluted 1:5) was recorded. For the calculation of the CEC the difference between the absorption of the Cu-triene solution (1:5) and the absorption of the supernatant of a sample is converted to the concentration and referred to the dry mass of the sample.

The CEC of the clay and the composition of the exchangeable cations are given in Table 3.2.

Table 3.2: Cation exchange capacity (CEC) and exchangeable cation composition of the studied Na- and Ca-bentonites, meq/100 g.

	CEC	Na^+	Ca^{2+}	K^++Mg^{2+}+Sr^{2+}
Na-bentonite	88	53.7	21.2	2.9
Ca-bentonite	87	0.0	76.7	2.0

3.6 Batch experiments

3.6.1 Immobilization of U(VI) on Na- and Ca-bentonites from $Ca(NO_3)_2$ and $NaNO_3$ solutions

The purpose of this series of batch experiments was to study the immobilization of U(VI) on Na- and Ca-bentonites from a $Ca(NO_3)_2$ solution, where the uncharged $Ca_2UO_2(CO_3)_3$ complex dominates the uranium speciation, as compared to a $NaNO_3$ solution, where the uranium speciation is dominated by a charged complex. Such a comparison was aimed at improving the understanding of the interaction of the $Ca_2UO_2(CO_3)_3$ complex with bentonite. The Na-bentonite samples consisted of original MX-80 bentonite with Na^+ being the predominating cation (86 %) in the interlayer space. For the Ca-bentonite samples, a certain quantity of the MX-80 bentonite was treated with a $CaCl_2$ solution, in order to obtain a homoionic Ca-clay.

For each sample, 1.5 g of clay were incubated with 30 ml of the tracer solution in glass vials. Two tracer solutions, 0.15 M $Ca(NO_3)_2$ and 0.3 M $NaNO_3$ solutions containing ~3.3 mM and ~3.6 mM $UO_2(NO_3)_2$, respectively, in combination with two bentonites, Na- and Ca-bentonites, were applied. In order to perform a time series for each of the four systems, multiples of identical samples had to be prepared, as the samples had to be discarded after the measuring procedure. Additionally, tracer solutions without clay (control) were measured for comparison. Minisart® Syringe Filters with a pore size of 200 nm and 20 nm were used to filter the supernatant solutions for analyses by ICP-AES and LIF. The experimental procedure in these batch-experiments is schematically presented in Fig. 3.3.

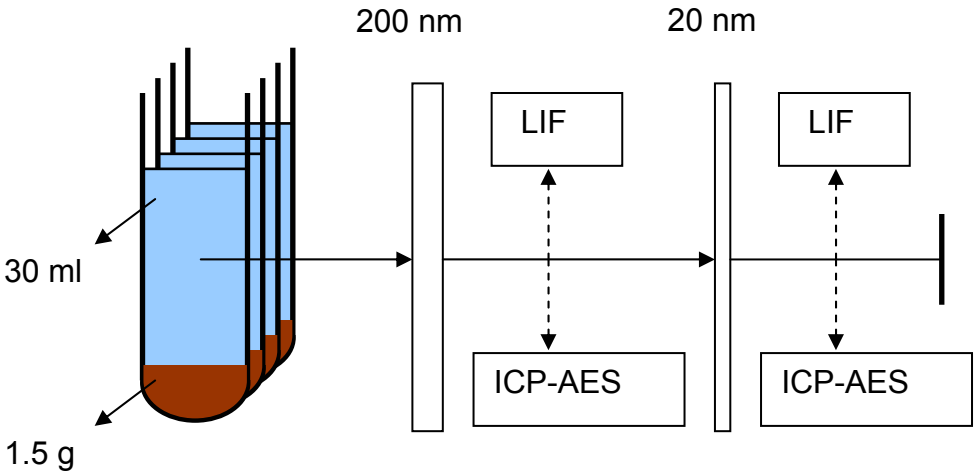

Fig. 3.3: Schematic of the experimental procedure in the batch-experiments.

The pH value of the solutions varied in the range between ~7.0 and 7.9 and was adjusted with Na_2CO_3 or $NaHCO_3$, if necessary. The duration of the experiment was set to 21 days based on the results of a preliminary trial study. Each sample was shaken for ~15 s once a day in the course of the experiment.

3.6.2 Effect of Ca^{2+} competition on U(VI) immobilization on Na- and Ca-bentonites

The purpose of this set of batch experiments was to study the effect of increasing Ca^{2+} concentrations and consequently of increasing concentrations of the $Ca_2UO_2(CO_3)_3$ complex on U(VI) immobilization on Na- and Ca-bentonites from a $NaNO_3$ solution of fixed ionic strength of ~0.26 M and in the pH range between 6.8 and 7.2. The same Na- and Ca-bentonites as in the batch experiments described above were used for sample preparation. However, as an important difference from that experiment, another solid-liquid ratio of 100 mg clay to 26.6 ml solution with a similar U(VI) concentration of 3.76 mM was applied. The amount of U(VI) in the supernatant solutions at this solid-liquid ratio corresponds to ~100 % of the CEC of the studied bentonites as compared to ~10 % of the CEC in the batch experiment described above. For each bentonite a series of seven samples with a Ca^{2+} concentration increasing from 0 up to ~25 mM in seven steps were incubated in glass vials for 21 days. The experimental procedure of these batch-experiments corresponds to that presented in Fig. 3.3.

3.7 Diffusion experiments

While batch-experiments exclusively elucidate interaction processes between solute and solid, as transport processes are minimized by mechanical means (suspending of the solid and intensive contact between solute and solid), diffusion tests are meant to demonstrate the overall retention effect of a solid on the solute by combining interaction and diffusion processes through a porous matrix. Transport effects may even prevail over interaction in case of highly dense materials.

Diffusion experiments have been carried out using five identical diffusion cells, made of PEEK, developed at and provided by KTH Stockholm (Fig. 3.4 and 3.5). The scheme of the experimental arrangement is shown in Fig. 3.6.

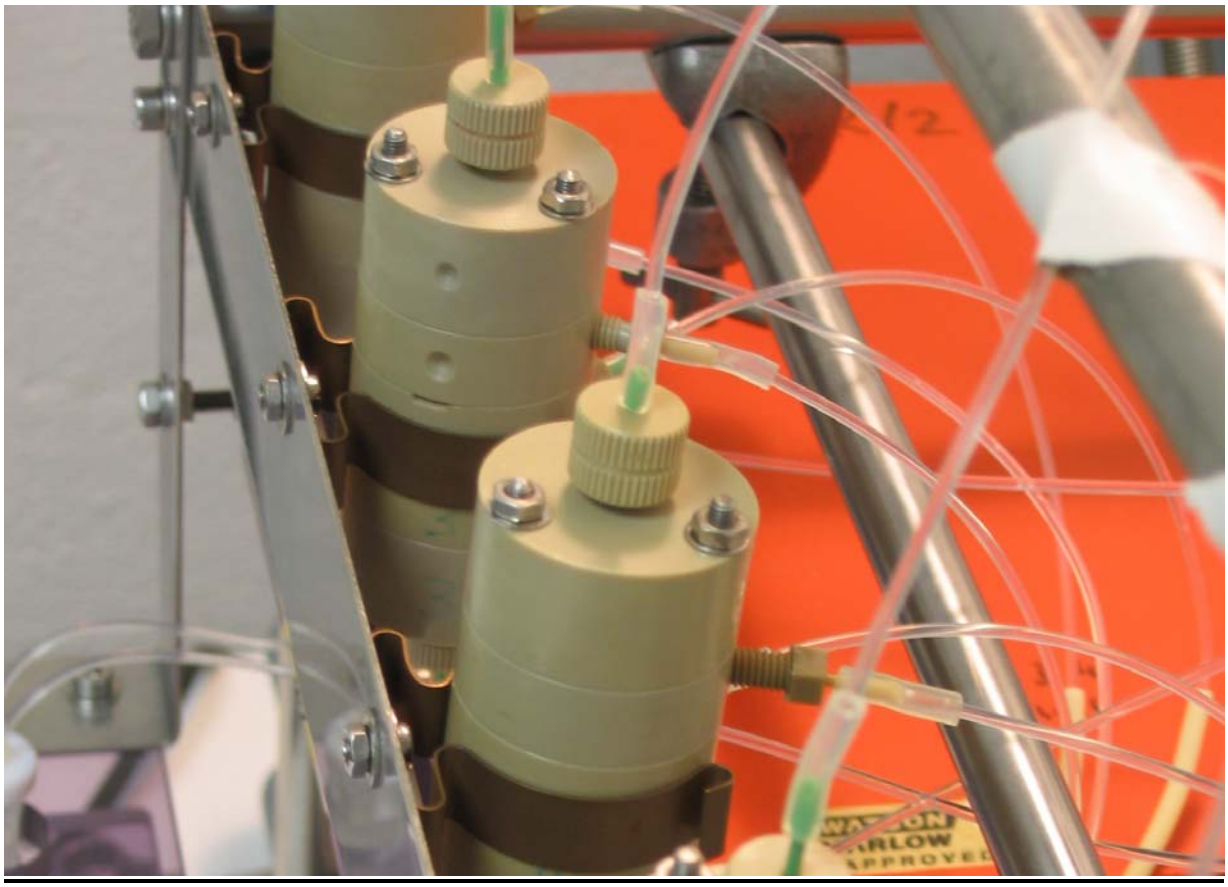

Fig. 3.4: Close-up of the diffusion cells and tubing

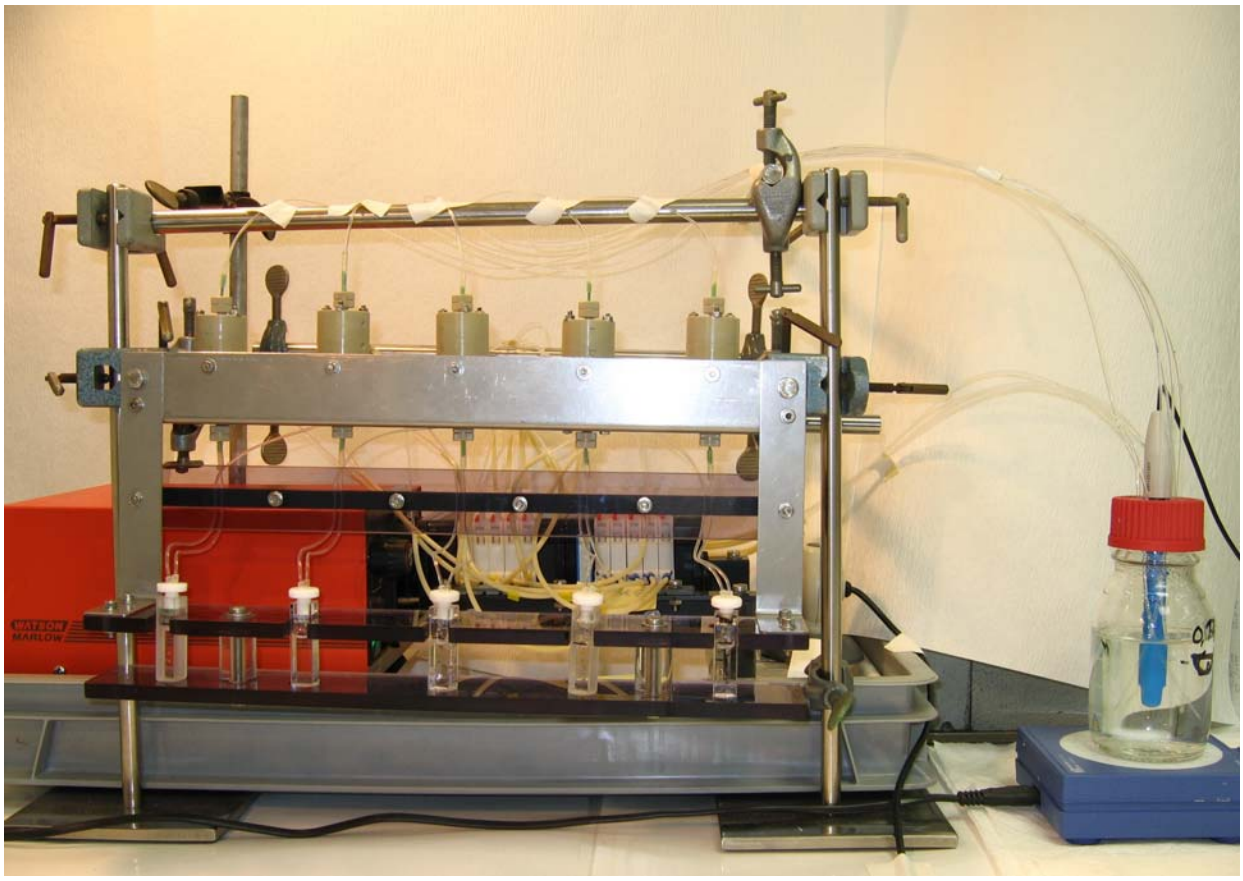

Fig. 3.5: Experimental set-up of the five diffusion cells (top row), the cuvettes (bottom row) and the solute reservoir (on the right) with the pH-probe.

All five cells are filled with Ca-bentonite, which is compacted in the diffusion cylinder to a dry density of 1.6 $g \cdot cm^{-3}$. The clay pellet has a diameter of 10 mm and a thickness of 5 mm. Stainless steel filters (0.82 mm thick) are fitted between the pellets and the endplates of the diffusion cells housing in- and outlet channels. The clay is saturated with the calcium nitrate equilibrium solution containing 0.15 mol l^{-1} Ca^{2+} for at least three weeks by circulating those uranium-free solutions from the solute reservoir and the cuvettes through the endplate channels by a peristaltic pump (Fig. 3.6). Extremely low pumping speeds are applied to avoid pressure gradients across the pellets.

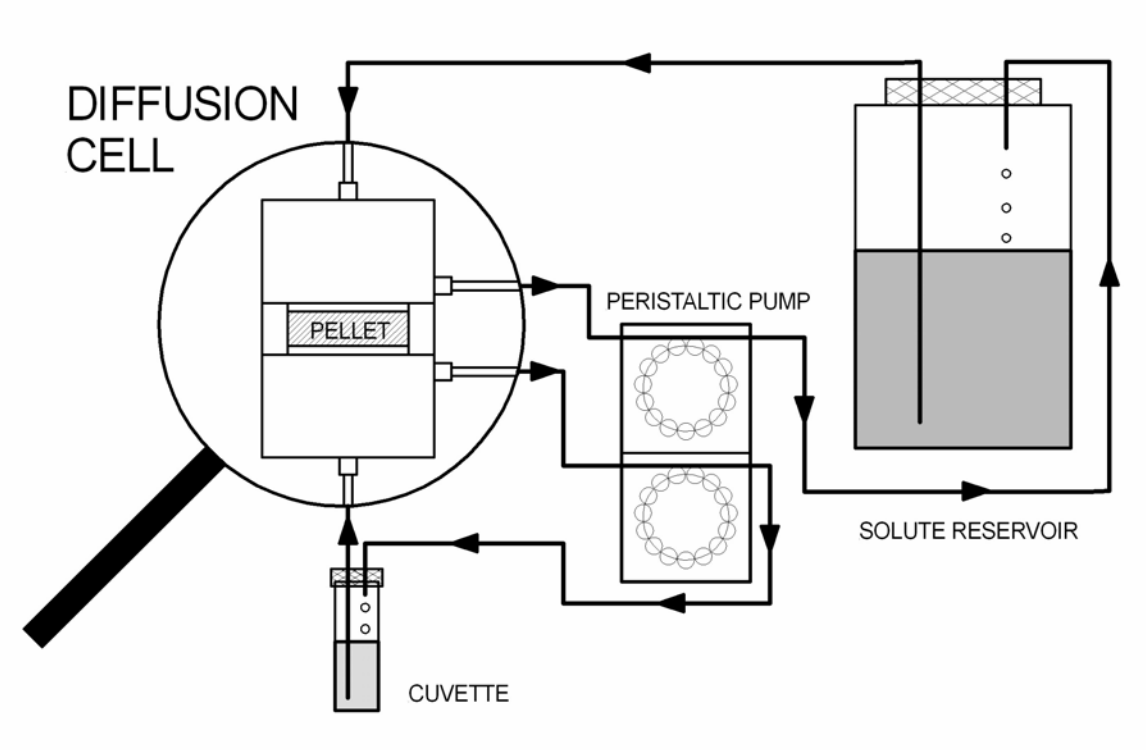

Fig. 3.6: Scheme of the experimental diffusion cell arrangement.

After equilibration, the solution in the solute reservoir is replaced by a $Ca(NO_3)_2$ solution containing 3.38 mM of uranyl, of which about 90 % are in the form of the $Ca_2UO_2(CO_3)_3$ aqueous complex, thus starting the diffusion process in all five diffusion cells at the same time. The pH-value of the solute reservoir is permanently controlled to ensure stability of the CaUC-complex. The solutions of the cuvettes are non-destructively analysed for the CaUC-complex by LIF measurements on a weekly basis.

4 Evaluation of experimental data and modelling

4.1 Evaluation of batch experiments

The kinetics of U(VI) uptake by Na- and Ca-bentonites (Na-Bt, Ca-Bt) from $Ca(NO_3)_2$ and $NaNO_3$ solutions is presented in Figure 4.1. It clearly shows that the type of the solution in contact with clay exerts a stronger effect on U(VI) uptake by clay than the type of clay does.

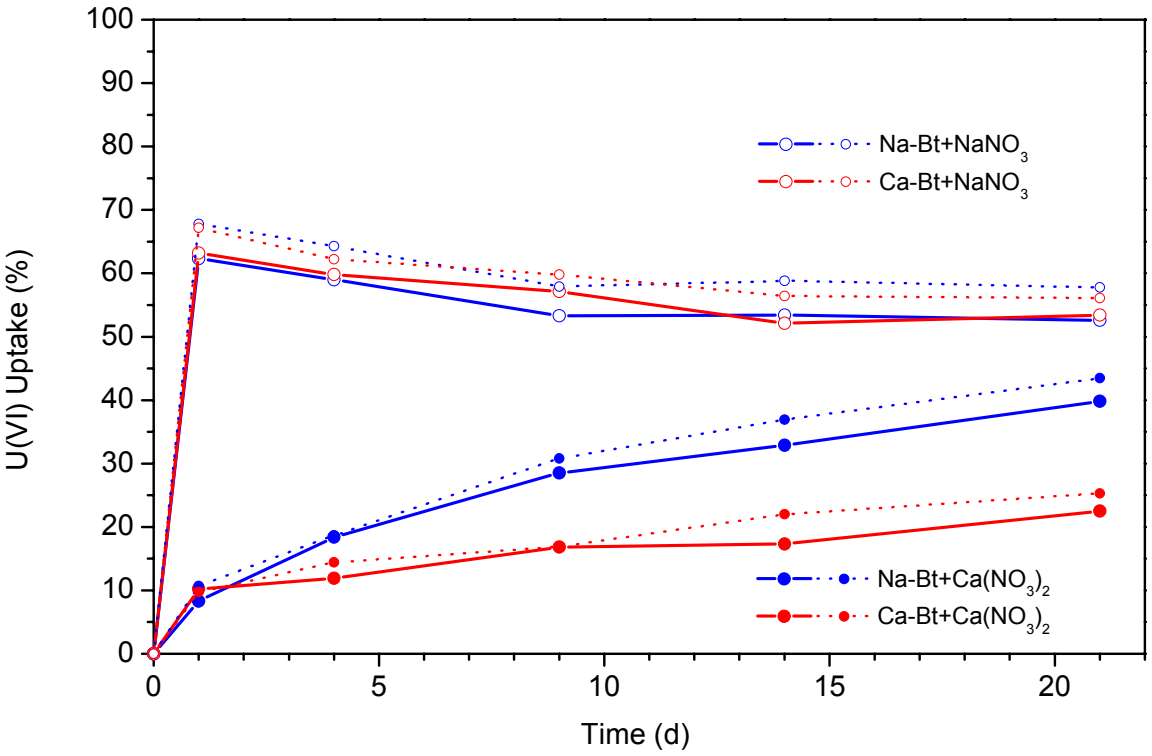

Fig. 4.1: Uranium (VI) uptake (in % of its initial dissolved amount) by Na- and Ca-bentonites from $Ca(NO_3)_2$ and $NaNO_3$ solutions after 200 nm (solid line) and 20 nm (dotted line) filtrations as a function of contact time.

This effect is manifested by very similar kinetics of U(VI) uptake from either $Ca(NO_3)_2$ or $NaNO_3$ solutions. Moreover, for a $NaNO_3$ solution, the extent of uptake is independent of the clay type. This is very different from the case with a $Ca(NO_3)_2$ solution, where Na-bentonite is able to immobilize about twice as much of uranium after 21 days of contact time than Ca-bentonite does. These observations indicate that immobilization of uranium on clay from aqueous solutions of higher ionic strength, is apparently determined by uranium speciation either in these solutions or at the clay-solution interface. This speciation, however, may change in respond to clay-solution interactions to favor uranium uptake as in the case of Na-bentonite in contact with a $Ca(NO_3)_2$ solution. The difference in the U(VI) speciation in the studied $Ca(NO_3)_2$ and $NaNO_3$ solutions at the circumneutral conditions of the experiment (7<pH<8) can be

best realized with help of the speciation diagrams in Figs. 4.2 and 4.3. These diagrams predict that U(VI) speciation is dominated by the charge neutral $Ca_2UO_2(CO_3)_3$ aqueous complex in a $Ca(NO_3)_2$ solution and by the negative hemicarbonate, $(UO_2)_2CO_3(OH)_3^-$, aqueous complex in a $NaNO_3$ solution. It follows then that whereas the latter negatively charged complex can apparently readily participate in the surface complexation at both Na- and Ca-bentonite interfaces, the neutral $Ca_2UO_2(CO_3)_3$ complex does not participate in such a complexation and as such prevents U(VI) immobilization on clay (Fig. 4.1). This conclusion is also supported by the comparison of the fraction of uranium immobilized from a $Ca(NO_3)_2$ solution on both clays after one day of contact time (~10%, Fig. 4.1) and of the fraction of uranium within the $(UO_2)_2CO_3(OH)_3^-$ aqueous complex in a $Ca(NO_3)_2$ solution (~10%, Fig. 4.2).

Fig. 4.1 also shows that the difference between U(VI) uptake on Na- and Ca-bentonites from a $Ca(NO_3)_2$ solution increases with time, so that about 20% and 40% of the initially dissolved uranium are immobilized on Ca- and Na-bentonites, respectively, after 21 days of contact time. On one hand, the time-depending increase of the extent of U(VI) immobilization indicates that it is specifically adsorbed in Na- and Ca-bentonites.

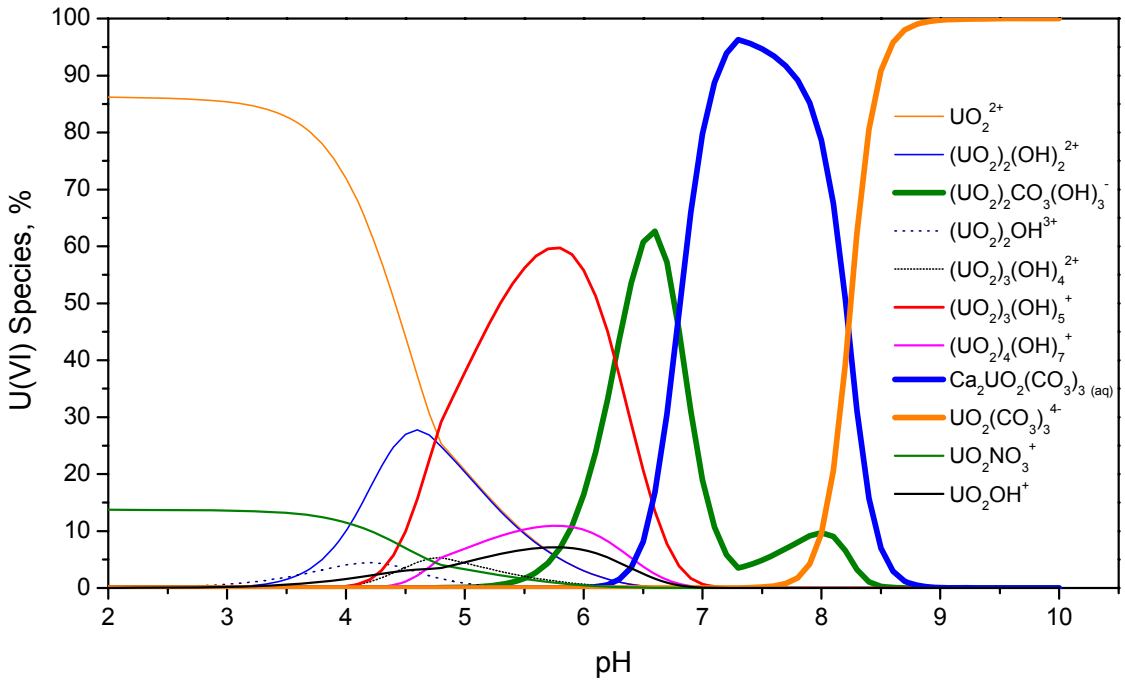

Fig. 4.2: Uranium (VI) speciation in a $Ca(NO_3)_2$ solution as a function of pH. The thermodynamic calculations were carried out with MINTEQA2 at the measured total alkalinity of ~525 mg/l.

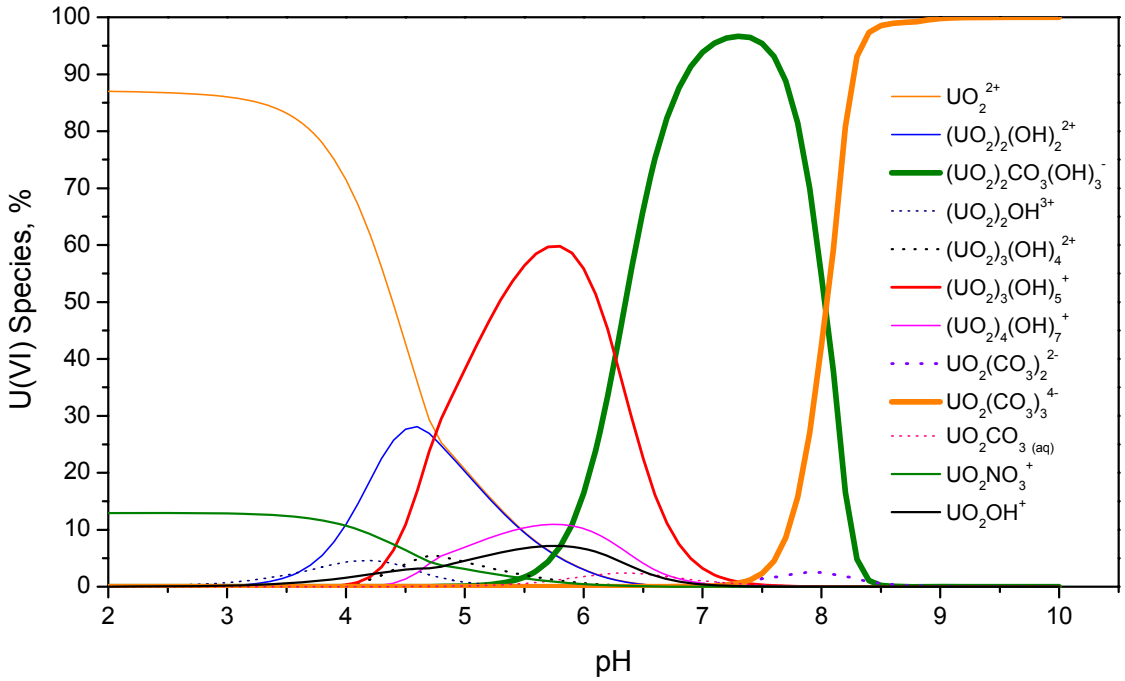

Fig. 4.3: Uranium (VI) speciation in a $NaNO_3$ solution as a function of pH. The thermodynamic calculations were carried out with MINTEQA2 at the measured total alkalinity of ~544 mg/l.

This is in agreement with the findings of previous studies on U(VI) interaction with swelling clay minerals which indicate that at circumneutral conditions it is preferentially adsorbed on the edge sites of montmorillonite and not in its interlayer spaces [Catalano and Brown, 2005]. On the other hand, since the fraction of uranium within the neutral $Ca_2UO_2(CO_3)_3$ complex makes about 90% of the total dissolved uranium in the $Ca(NO_3)_2$ solution, the U(VI) immobilization above the 10% value means also that there is some mechanism causing destruction of the $Ca_2UO_2(CO_3)_3$ complex at the bentonite interface, which is more effective for Na-bentonite as compared to Ca-bentonite. The effect of this mechanism cannot be attributed to a Ca depletion of the $Ca(NO_3)_2$ solution, because firstly, the studied Na-bentonite is able to adsorb at most ~27 mmol/l of Ca (*e.g.*, as $CaCl^+$ pairs) through ion exchange (see Table 3.1), which is much less than the Ca concentration in the $Ca(NO_3)_2$ solution (~150 mmol/l), and secondly, it takes place also for Ca-bentonite, where no Ca-depletion due to sorption on bentonite can be expected. This effect should then be attributed to a continuous uranium depletion of the aqueous solution in contact with clay. Since U(VI) in $Ca_2UO_2(CO_3)_3$ complexes cannot interact directly with clay, such a depletion is in turn only possible, if a continuous shift of the thermodynamic equilibrium favouring complex destruction takes place in the solution. Indeed, as a result of the immobilization of U(VI) being initially not in the $Ca_2UO_2(CO_3)_3$ complex (~10%, Fig. 4.2), the re-establishing of the shifted thermodynamic equilibrium in the solution requires a redistribution of the remaining dissolved U(VI) according to its initial speciation. After com-

pletion of this redistribution, ~90% of the dissolved U(VI) occurs as $Ca_2UO_2(CO_3)_3$ complex, the remainder being available for immobilization. A sequence of such "uranium immobilization" – "complex destruction" cycles apparently leads to the observed kinetics of U(VI) uptake from a $Ca(NO_3)_2$ solution. The validity of the suggestion about the uranium depletion in the $Ca(NO_3)_2$ solutions in contact with clay was confirmed in our experiment through an addition of dissolved U(VI) (as $UO_2(NO_3)_2$) to the $Ca(NO_3)_2$ supernatant solutions in amounts compensating its uptake by clay, which led to a re-establishing of the initial concentration of $Ca_2UO_2(CO_3)_3$ species estimated from the values of its integral fluorescence intensity. The data on time-dependent changes in this measurable characteristics of supernatant solutions confirm also the related suggestion about the continuous decline of $Ca_2UO_2(CO_3)_3$ concentration as a result of progressive "uranium immobilization" – "complex destruction" cycles (Fig. 4.4).

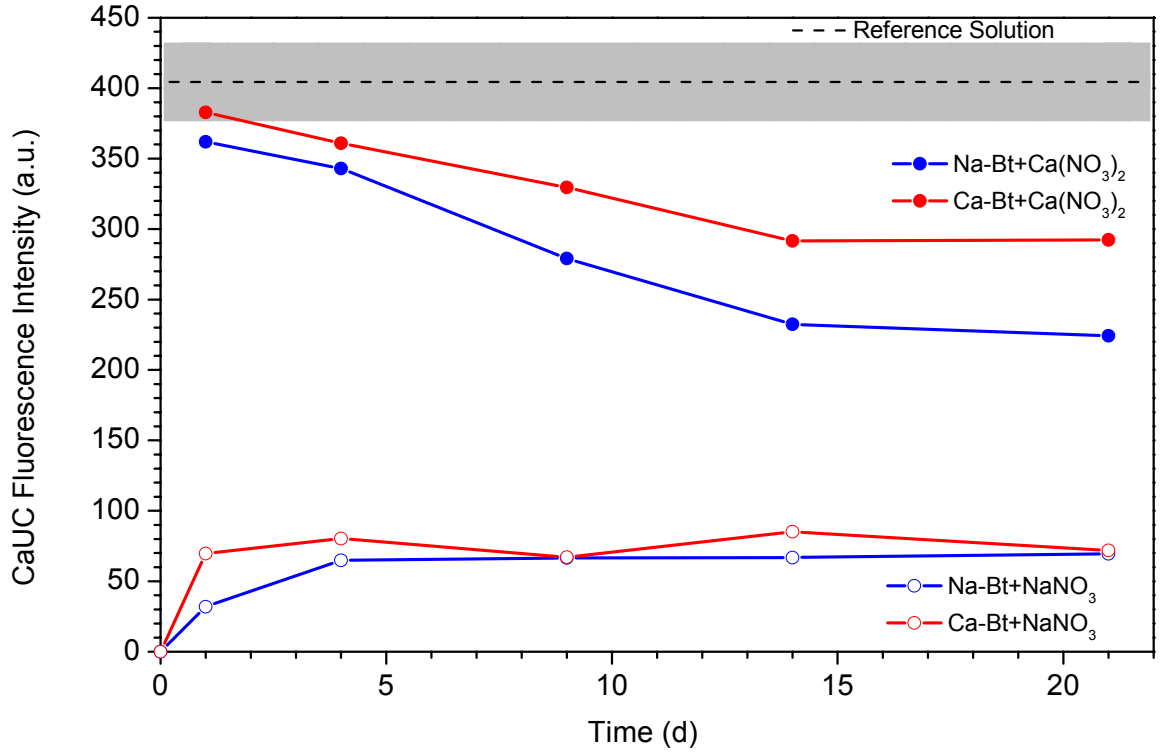

Fig. 4.4: Integral laser induced fluorescence of the $Ca_2UO_2(CO_3)_3$ complex in supernatant $Ca(NO_3)_2$ and $NaNO_3$ solutions after contact with Na- and Ca-bentonites as a function of contact time.

Figure 4.4 shows that the integral fluorescence intensity of $Ca_2UO_2(CO_3)_3$ in a $Ca(NO_3)_2$ supernatant solution decreases by ~20% and ~40% after 21 day of contact time with Ca- and Na-bentonites, respectively. These values are in perfect agreement with the corresponding values on uranium uptake by these clays (Fig. 4.1). Further-

more, the difference between the values of integral fluorescence intensity for Ca- and Na-bentonites increases with time the same way as the difference in U(VI) uptake from a $Ca(NO_3)_2$ solution in contact with these clays does (Fig. 4.1).

Additionally, two highly important findings based on the data in Figure 4.4 are, firstly, that $Ca_2UO_2(CO_3)_3$ species is formed in the initially Ca-free $NaNO_3$ solution after one day of contact with either Na- or Ca-bentonite due to an obvious Ca-release from the clay and, secondly, that its concentration remains approximately constant during the experiment. From these data, $Ca_2UO_2(CO_3)_3$ species can be estimated to account for ~15% of the initial amount of dissolved U(VI) in the $NaNO_3$ solution. However, considering that at the same time about 60% of the initially in this solution dissolved U(VI) are immobilized by bentonites, $Ca_2UO_2(CO_3)_3$ accounts for ~50% of the remaining dissolved U(VI), which is an extremely high value for the solution with initially no $Ca_2UO_2(CO_3)_3$ species at all (Fig. 4.3).

Considering the average pH value of ~7.6 for the $NaNO_3$ solution in contact with Na- and Ca-bentonites, the conclusion discussed above that the $(UO_2)_2CO_3(OH)_3^-$ complex readily interacts with clay interfaces and the fact that at this pH value $UO_2(CO_3)_3^{4-}$ and $UO_2(CO_3)_2^{2-}$ species account for between 10% and 20% of the total dissolved U(VI), it can be concluded that these species are precursors of the newly formed $Ca_2UO_2(CO_3)_3$ complex. Moreover, it follows necessarily from this fact that the latter complex has a higher formation constant at the conditions of the experiment than the di- und tri-carbonate uranyl complexes have, which supports the guide values for these constants as discussed by Guillaumont *et al.*, 2003. Furthermore, the observation that the amount of the $Ca_2UO_2(CO_3)_3$ complex newly formed in the $NaNO_3$ solution practically does not change as opposed to the case with the $Ca(NO_3)_2$ solution (Fig. 4.4), allows to draw the conclusion that interaction of the $(UO_2)_2CO_3(OH)_3^-$ complex with clay leads to a rapid (within at maximum one day) and irreversible neutralization of the reactive sites responsible elsewise for the time-dependent U(VI) adsorption at the clay interface from the $Ca(NO_3)_2$ solution (Fig. 4.1). In this relation, the slower kinetics of U(VI) immobilization from a $Ca(NO_3)_2$ solution on Ca-bentonite as compared to that for Na-bentonite indicates that some surface complexes specific to Ca-bentonite are able to effectively, albeit not irreversibly, neutralize the reactive sites responsible for U(VI) adsorption.

Along with the retention ability of clay with respect to the dissolved uranium discussed above, another important aspect of uranium transport in a porous medium has been treated in our batch experiments. All supernatant solutions were successively filtrated with filters of 200 nm and 20 nm pore sizes, in order to identify a possible uranium association with fine-sized colloids. The data in Fig. 4.1 reveal that after 21 days of contact time at the applied experimental conditions about 5% and 10%

of the supernatant U(VI) can be considered as associated with fine colloids of size >20 nm and <200nm for $Ca(NO_3)_2$ and $NaNO_3$ solutions, respectively. The difference in the amounts of colloid-associated U(VI) for these two solutions can obviously be attributed to the stronger ability of Ca^{2+} to compete with dissolved uranyl species for the sorption sites at the colloidal interface as compared to that of Na^+. An exact mineralogical identification of these colloids is only possible with help of a thorough and rather complicated experimental procedure. Still, the fact that no Fe and Al were detected in the size fraction >20 nm and <200nm allows to discard the suggestion about their aluminosilicate, alumino- or iron-(hydr)oxide origin. Furthermore, their presence in the Ca-poor $NaNO_3$ solution indicates that they are not of calcium carbonate origin. Indeed, out of the chemical elements detected with help of ICP-AES, only silica was affected by the applied filtration procedure in all four studied systems as represented in Fig. 4.5. This observation allows to suggest that a fraction of dissolved U(VI) is adsorbed on the colloidal amorphous silica, which can account for up to several weight percents in Wyoming bentonite [Metz *et al.*, 2005].

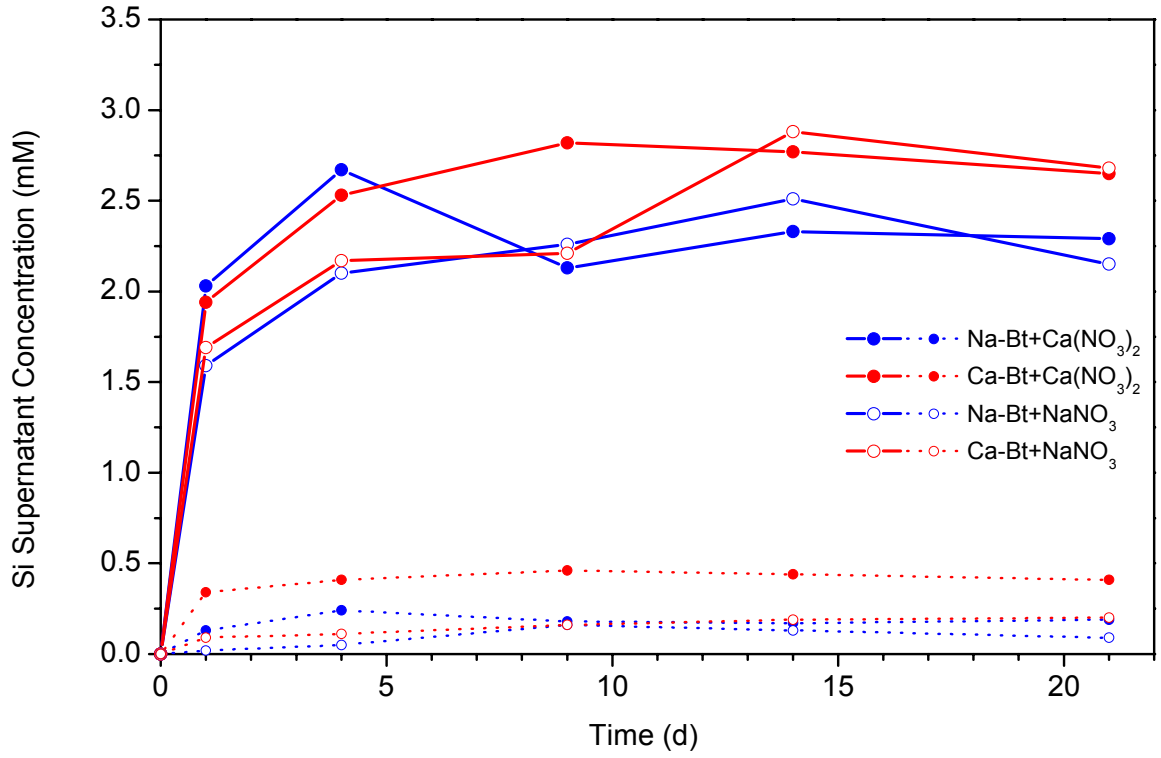

Fig. 4.5: Silica concentrations in supernatant $Ca(NO_3)_2$ and $NaNO_3$ solutions after contact with Na- and Ca-bentonites as well as after 200-nm (solid line) and 20-nm (dotted line) filtrations as a function of contact time.

The interaction of the dissolved U(VI) with the amorphous silica seems, however, to be of very different nature for $Ca(NO_3)_2$ compared to $NaNO_3$ solutions according to

the comparison of the LIF spectra presented in Figs. 4.6 and 4.7. Whereas no effect of the 20 nm filtration on the LIF-spectrum can be seen for the $Ca(NO_3)_2$ solution, there is a pronounced effect for the $NaNO_3$ solution. Taking into account the fact that the removal of about 5% of U(VI) from the $Ca(NO_3)_2$ solution on 20 nm filtration is not accompanied by a decrease of the LIF intensity, the conclusion can be made that uranyl associated with amorphous silica colloids is complexed with ligands quenching its fluorescence at ambient temperature. Since surface complexation of uranyl with silica does not lead to a quenching of uranyl fluorescence [Lopez and Birch, 1996], it can then be supposed that the quenching ligands within the surface species of uranyl at the silica interface in the $Ca(NO_3)_2$ solution originate from the solution (e.g. carbonate, chloride ions). The fact that the fluorescence of an uranyl surface species at the silica interface is not quenched in a $NaNO_3$ solution (Fig. 4.7) allows to conclude that this species has a different composition than the surface species in the $Ca(NO_3)_2$ solution. Furthermore, this difference cannot be due to the participation of Na^+ or Ca^{2+} as ligands in this complex, since the uranyl fluorescence would not be quenched in this case.

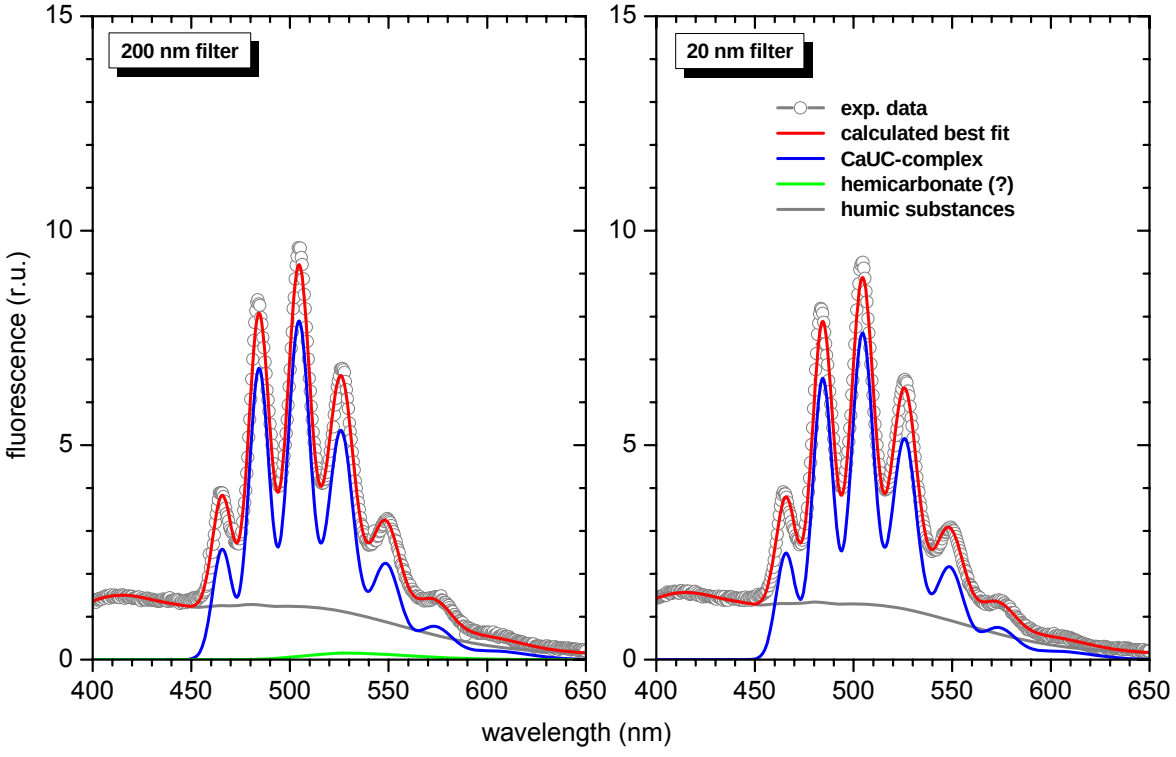

Fig. 4.6: Effect of 20 nm filtration on the fluorescence spectra of uranyl species in the supernatant $Ca(NO_3)_2$ solution after contact with Na- or Ca-bentonite (filtration effect is identical for both clays).

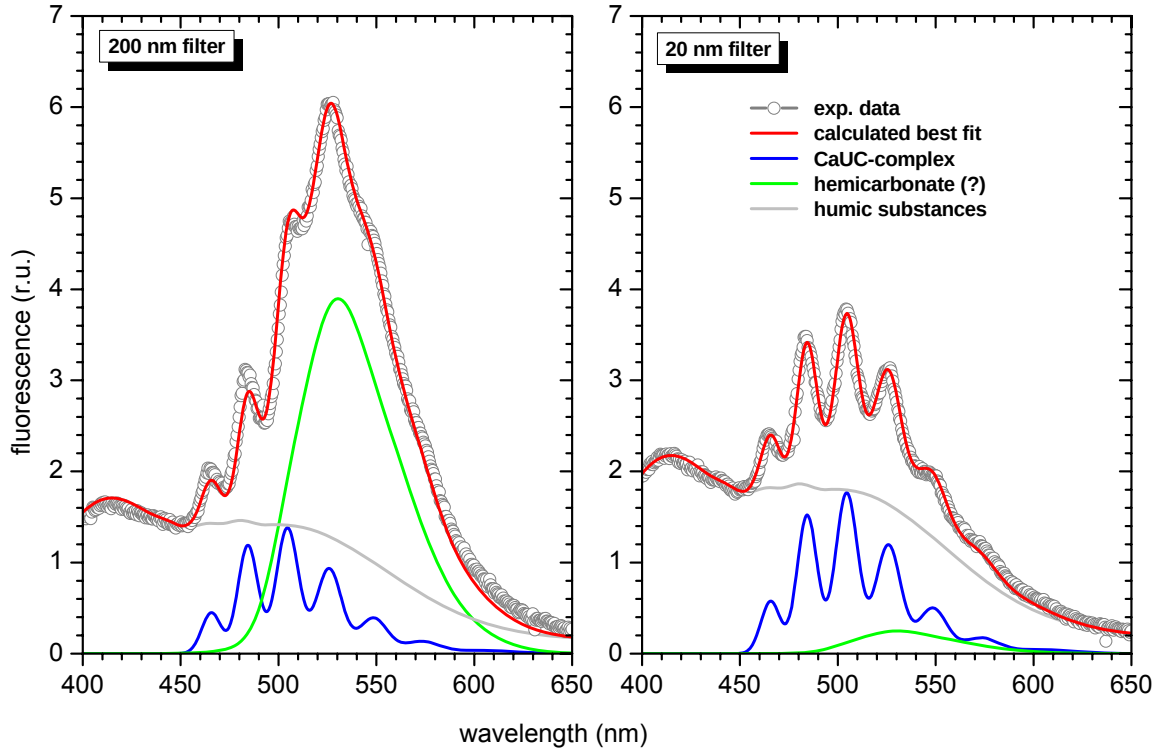

Fig. 4.7: Effect of 20 nm filtration on the fluorescence spectra of uranyl species in the supernatant $NaNO_3$ solution after contact with Na- or Ca-bentonite (filtration effect is identical for both clays).

The effect of Ca-competition on U(VI) immobilization on Na- and Ca-bentonites is represented in Fig. 4.8. This figure shows that the conclusion about the prevalence of the type of the solution in contact with clay to the type of clay with respect to the exerted effect on U(VI) uptake is apparently valid only for [U]/([U]+[Ca]) ratios below ~0.5. Such ratios should be expected in most natural waters. However, for some generally less probable but - due to human activity - possible ratios above ~0.5, just the opposite prevalence is true. In this range, Na-bentonite shows a significantly higher preference for U(VI) as compared to Ca than Ca-bentonite does. Moreover, for the ratios above ~0.8, Na-bentonite can apparently supply some reactive sites, which are highly selective to U(VI) as compared to Ca. No such reactive sites are available for U(VI) in Ca-bentonite. It is noteworthy that at ratios in the range between ~0.4 and ~0.8, Ca-bentonite shows as well some preference for U(VI) as compared to Ca. Such a preference prevents an increase in the extent of the formation of $Ca_2UO_2(CO_3)_3$ complex in the solution despite the increasing Ca concentration, as can be seen in Fig. 4.9. In agreement with data on U(VI) uptake, this figure shows that the concentration of $Ca_2UO_2(CO_3)_3$ complex is generally higher in contact with Ca-bentonite as compared to Na-bentonite.

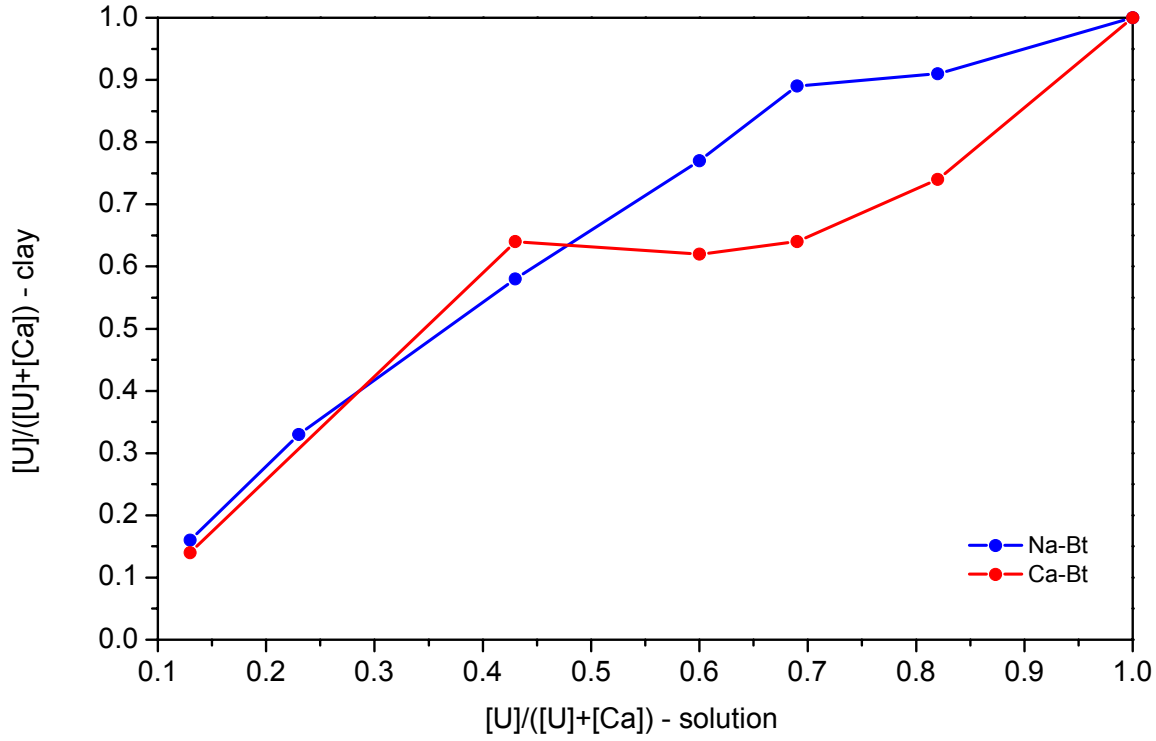

Fig. 4.8: Relative fraction of U(VI) immobilized on clay as a function of the applied relative fraction of U(VI) in solution (~200<[$NaNO_3$]<~250 mM, 0<[$Ca(NO_3)_2$]<~25 mM, [$U(NO_3)_2$] = 3.76 mM).

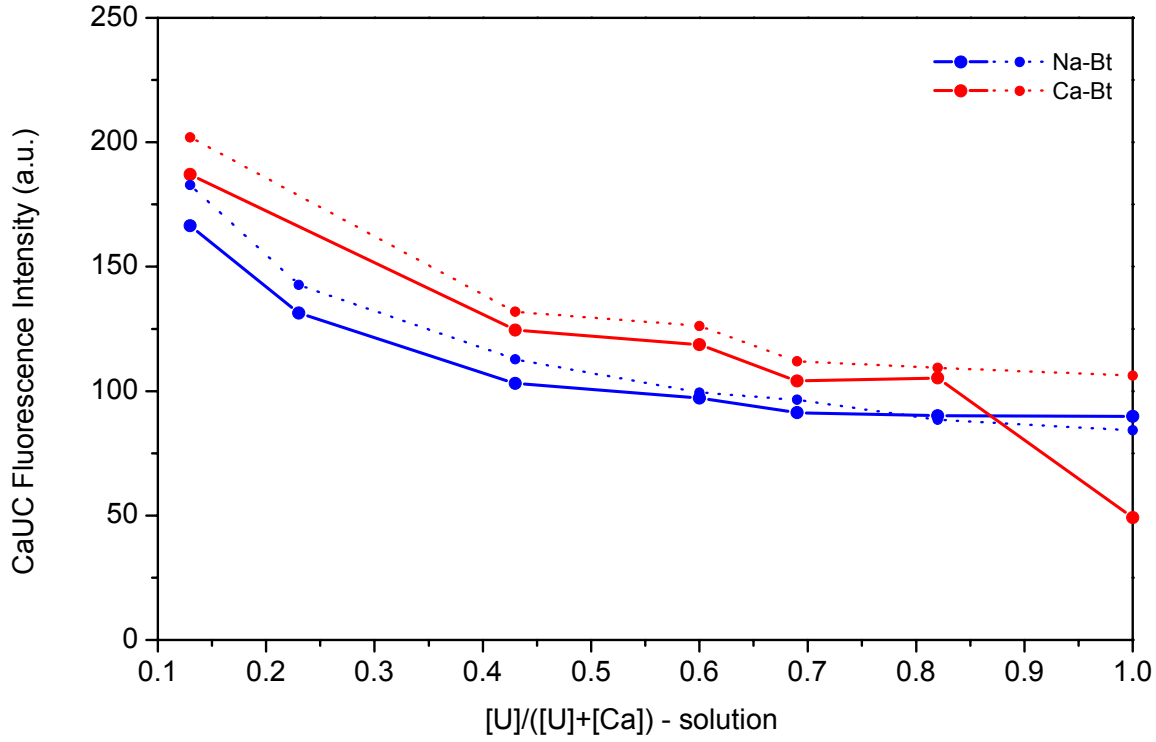

Fig. 4.9: Integral fluorescence intensity of the $Ca_2UO_2(CO_3)_3$ complex after 200 nm (solid line) and 20 nm (dotted line) filtrations as a function of the applied relative fraction of U(VI) in solution (~200<[$NaNO_3$]<~250 mM, 0<[$Ca(NO_3)_2$]<~25 mM, [$U(NO_3)_2$] = 3.76 mM).

Differently from the dissolved uranyl species in the supernatant solutions, uranyl species immobilized on the Na- or Ca-bentonites from a $Ca(NO_3)_2$ solution show no spectral signature characteristic for the aqueous $Ca_2UO_2(CO_3)_3$ complex or its crystalline counterpart, synthetic liebigite (Fig. 4.10 spectrum A and spectrum B). This observation supports the conclusion made above based on U(VI) immobilization data (Fig. 4.1) that the $Ca_2UO_2(CO_3)_3$ complex is not immobilized on clay. The species immobilized on bentonite is characterized by the absence of the two higher-energetic vibration bands of the electronic ground state, which suggests a strong structural distortion in its excited electron state (Fig. 4. 10 spectrum B). The identical spectral signature was observed for uranyl species adsorbed on SWy-1 smectite by Chisholm-Brause *et al.* [2004] (Fig. 4. 10 spectrum C), which supports the consideration of the montmorillonitic component of bentonite as the main immobilization sink for dissolved U(VI) in contacting solutions.

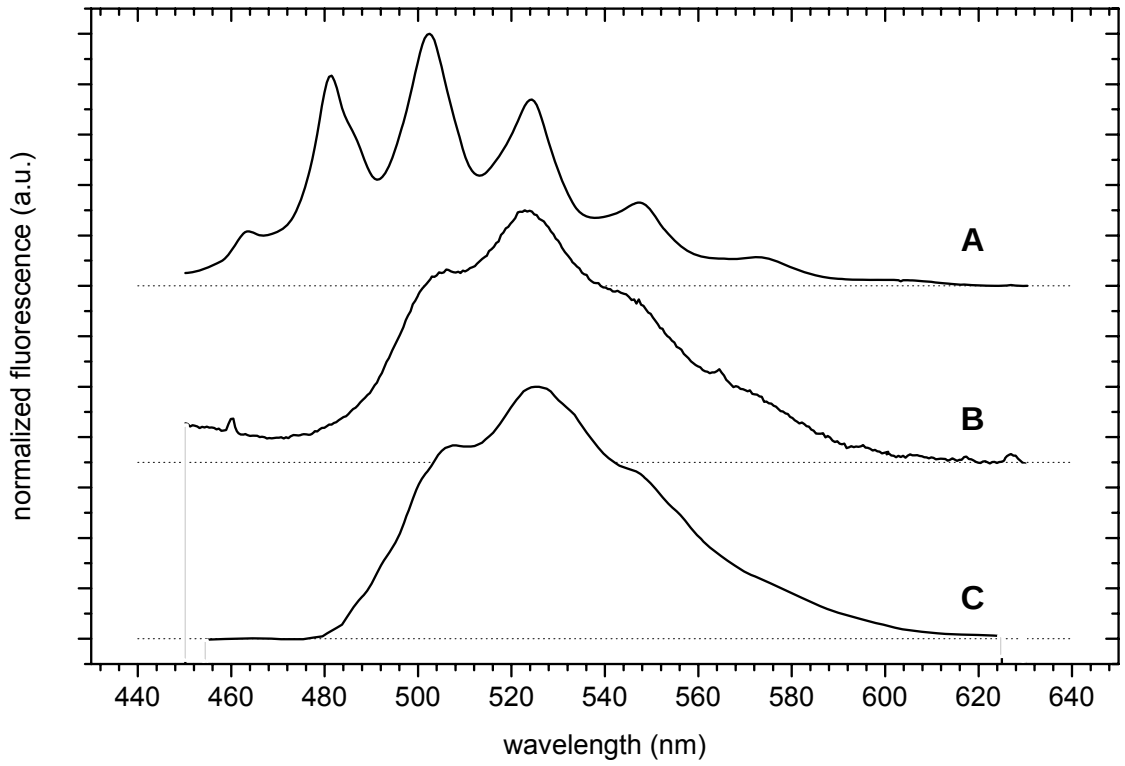

Fig. 4.10: Fluorescence spectra for a synthetic liebigite, $Ca_2UO_2(CO_3)_3 \cdot 10H_2O$ (A), air-dried Na- and Ca-bentonites after contact with a $Ca(NO_3)_2$ solution (spectra are identical for both clays) (B) and a reference smectite SWy-1 after contact with U(VI)-containing solution [Chisholm-Brause *et al.*, 2004] (C). All spectra have been normalized to maximum intensity to facilitate comparison.

Additional information about the surface distribution of uranyl species immobilized on bentonite can be obtained from the observation of the effect of the re-wetting of the air-dried bentonite samples on the fluorescence signature of this species as represented in Fig. 4.11. The fluorescence intensity increasing as a function of reaction time can indicate either (1) mobilization of the adsorbed uranyl species and their diffusion-mediated polymerization or (2) the advance of the hydrolysis reactions leading to an increase of the number of OH ligands of adsorbed uranyl species, as also suggested in other studies [Chisholm-Brause *et al.*, 2004]. Still, the time scale of the reaction in Fig. 4.11 (from few minutes up to one hour and more) strongly favours rather the first hypothesis, which allows to draw the conclusion that uranyl species do not polymerize during immobilization.

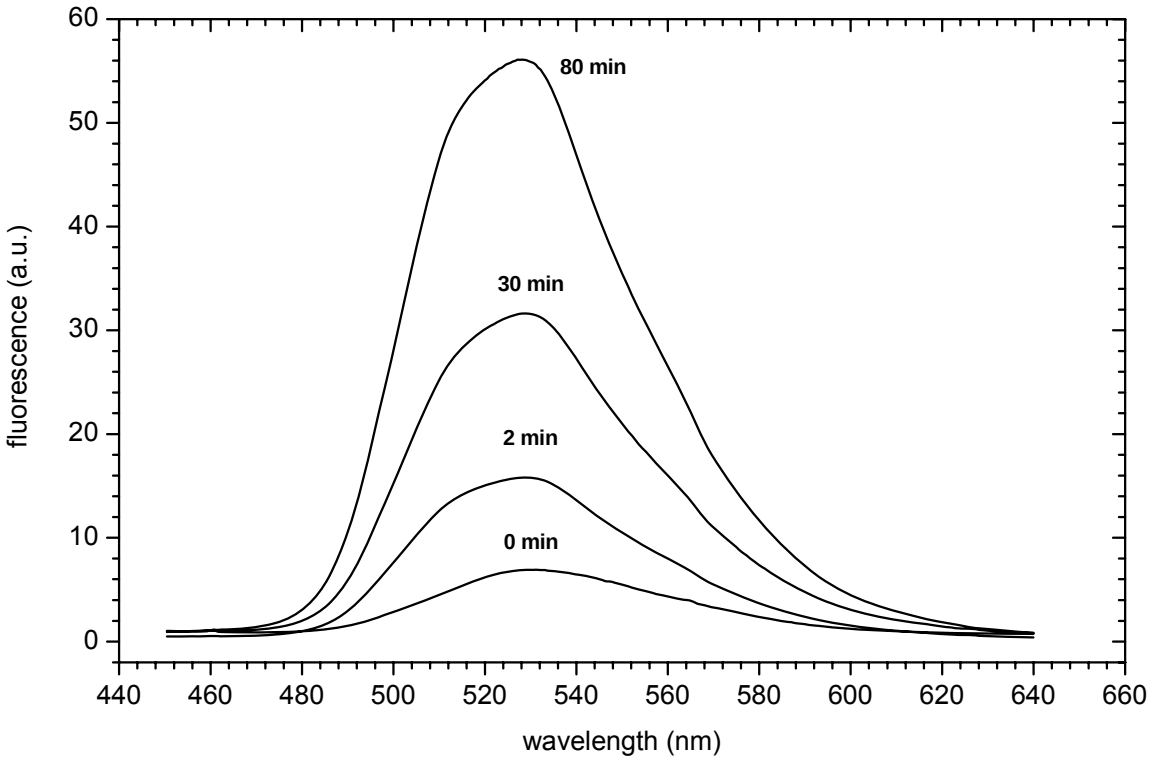

Fig. 4.11: Effect of a re-wetting with MilliQ water of the air-dried Na- and Ca-bentonites after contact with a $NaNO_3$ solution as a function of reaction time (fluorescence spectra are identical for both clays).

4.2 Evaluation of the diffusion experiments

After 196 days, no $Ca_2UO_2(CO_3)_3$ complex could be identified by LIF in the cuvette solution of the diffusion cell experiment. However, ICP-MS analysis of this solution showed a uranium concentration of about 0.25 % of that of the reservoir solution. Converting this uranium concentration into that of the CaUC complex would mean that LIF measurements should have been able to identify the complex. Since they did not, it is assumed that the uranium speciation has changed during passage through the clay pellet.

Two diffusion cells were disassembled after 196 days, and the pellets were cut vertically into two half cylinders each. The cross sections were scanned by micro-XRF measuring points in a 50 (depth) times 60 (width) point grid. As shown in Figs. 4.11 (clay pellet No. 3) and 4.13 (clay pellet No. 5), which are very similar, the uranium front has not moved more than 0.5 mm during the 28-week diffusion time. However, individual uranium spots can be seen throughout the pellet down to the lower end.

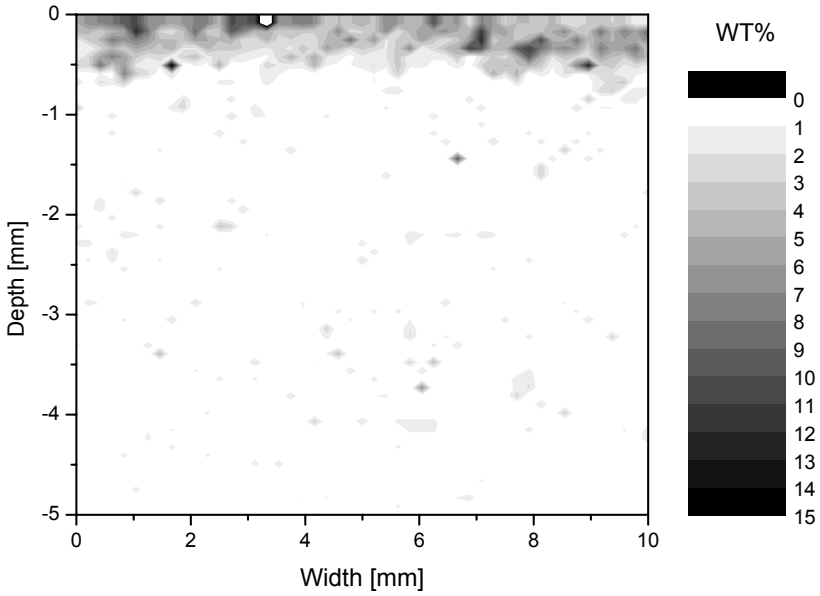

Fig. 4.11: Micro-XRF scan of the total vertical cross section of Ca-bentonite pellet No. 3 after a 196-day diffusion period. Grid of measuring points: 50 in depth x 60 in width, measuring time: 200ms per measuring point.

A vertical line scan with longer measuring times along the center of the cross section yields the vertical uranium distribution, as given in Fig. 4.12 (clay pellet No. 3). It quantifies the qualitative evidence of a slowly moving concentration front and the appearance of minute amounts of uranium at the lower and of the pellet.

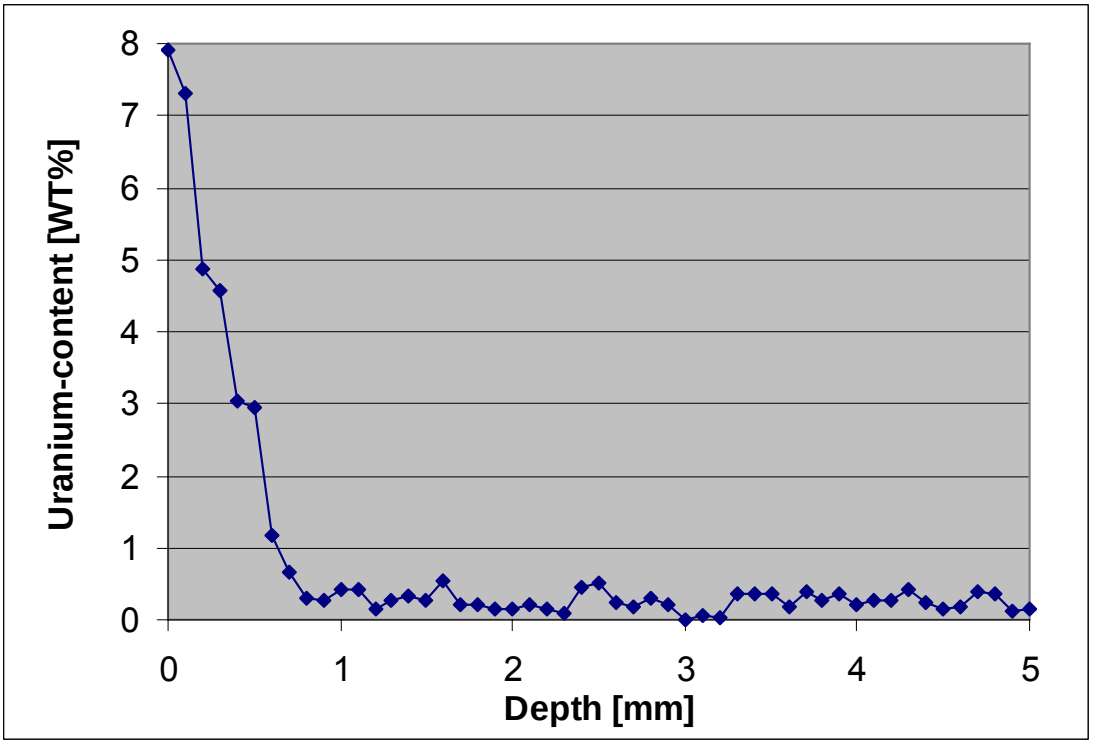

Fig. 4.12: Micro-XRF vertical line scan of the center of Ca-bentonite pellet No. 3 after a 196-day diffusion period. 60 measuring points in depth, 30 s measuring time per point.

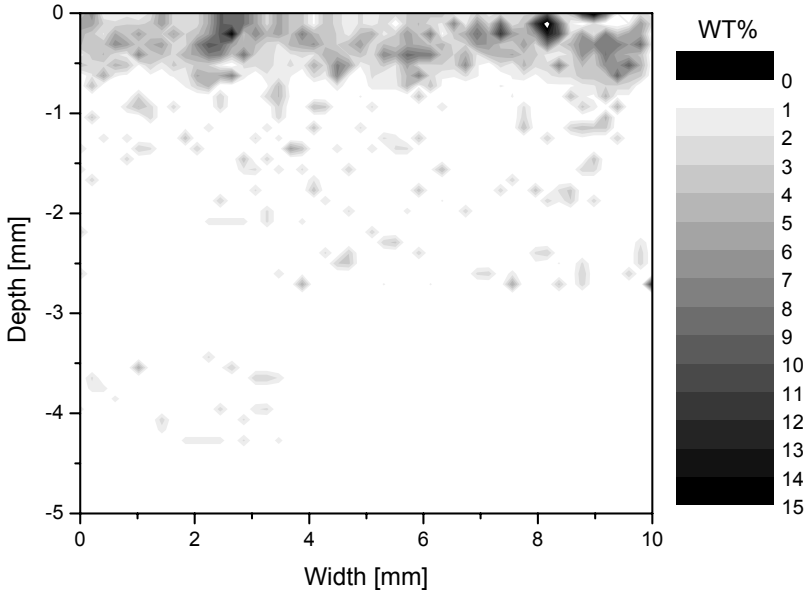

Fig. 4.13: Micro-XRF scan of the total vertical cross section of Ca-bentonite pellet No. 5 after a 196-day diffusion period. Grid of measuring points: 50 in depth x 60 in width, measuring time: 200 ms per measuring point.

Figure 4.14 (clay pellet No. 5) shows two vertical line scans, one performed along the center line and, for comparison, one performed along the outside cylindrical surface of the pellet. These two scans confirm the homogeneous progression of the uranium front and the fact that no fringe effects concerning uranium movement occur in the clay pellet.

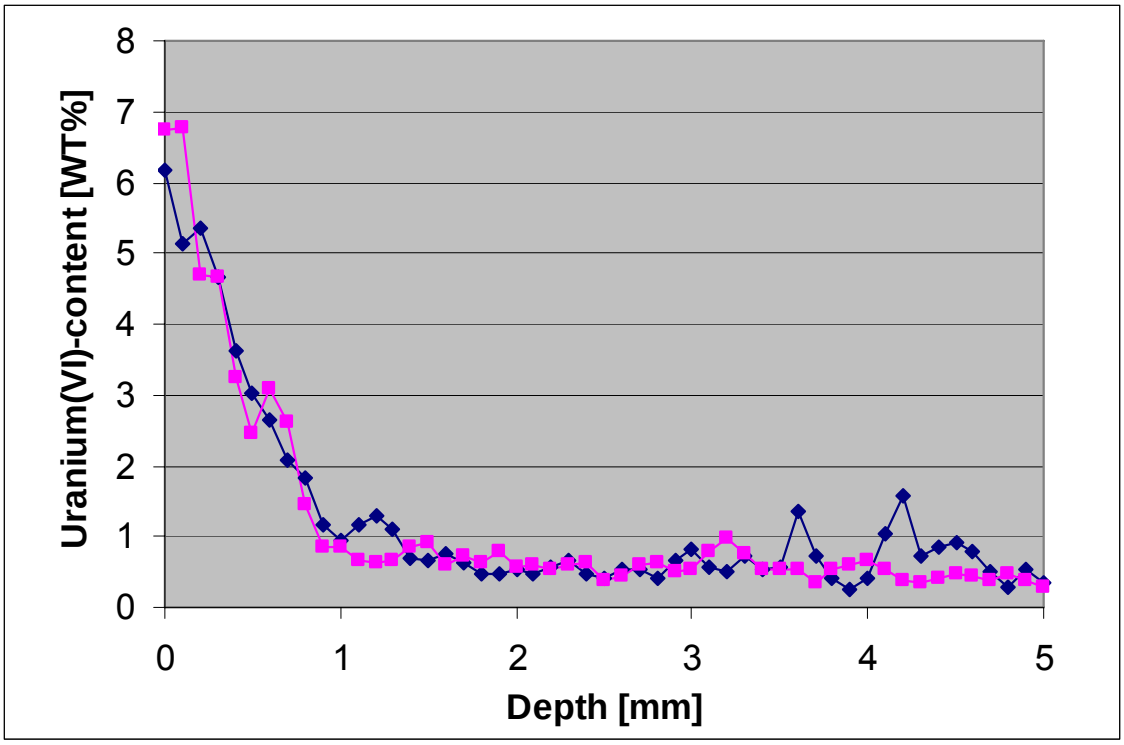

Fig. 4.14: Two micro-XRF vertical line scans of Ca-bentonite pellet No. 5 after a 196-day diffusion period. 60 measuring points in depth, 30 s measuring time per point. Blue line: Vertical scan in the center; Red line: Vertical scan on the outside cylindrical surface of the pellet.

In agreement with micro-XRF data, figure 4.16 shows that uranyl species have migrated through the pellet and have reached its bottom surface. However, no spectral signature characteristic for the CaUC complex could be detected, neither within the pellet nor in the outlet cuvette. The reason for this observation could be the high constrictivity of the bentonite pellet at the rather high density of 1.6 g/cm^3, so that a relatively large CaUC species with the equatorial diameter of ~1 nm has not diffused inside the pellet within the experiment duration. Indeed, it can be suggested from the above figure that only a subset of the uranyl species present at the top surface of the pellet diffuses inside the pellet. It is noteworthy, that the spectral signature inside the pellet shows close similarities to that measured for uranyl species immobilized on the bentonite surface in the batch experiments (Fig. 4.10 spectrum B). This suggests that

batch experiments may adequately represent interaction reactions also valid during diffusion processes.

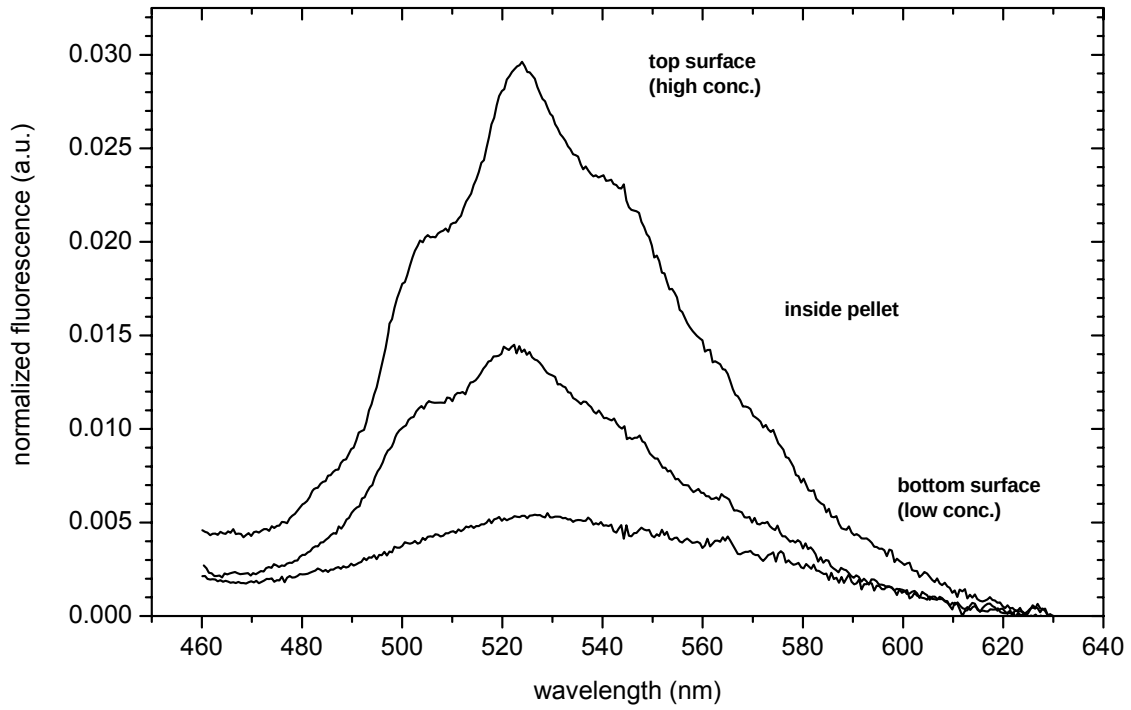

Fig. 4.16: LIF spectra obtained on different sides of the bentonite pellet after finishing the diffusion experiment (196 days). From upper to lower curve: Emission measured at the top surface of the pellet in contact with the tracer solution containing the CaUC complex, inside the pellet after diffusive transport of uranyl species, at the bottom surface in contact with the $Ca(NO_3)_2$ solution of the cuvettes.

5 Conclusions

- The $Ca_2UO_2(CO_3)_{3\ (aq)}$ concentration decreases by up to ~40% as a result of interaction with Na-bentonite.

- Immobilization of U(VI) is a factor of ~2 lower for solutions with the uncharged $Ca_2UO_2(CO_3)_{3\ (aq)}$ complex dominating the U(VI) speciation as compared to solutions, where it is dominated by negatively charged U(VI) complexes.

- Ca-bentonite is characterized by a factor of ~2 lower immobilization ability for U(VI) than Na-bentonite is for solutions with $Ca_2UO_2(CO_3)_{3\ (aq)}$ dominating the U(VI) speciation.

- Under the applied experimental conditions, about 5% and 10% of the supernatant U(VI) is associated with silica colloids of sizes >20 nm and <200nm for $Ca(NO_3)_2$ and $NaNO_3$ solutions, respectively.

- About 15% of the initially dissolved U(VI) are complexed in the highly mobile $Ca_2UO_2(CO_3)_{3\ (aq)}$ species as a result of Ca-release from Na- or Ca-bentonites into the initially Ca-free U(VI)-containing solution.

- The $Ca_2UO_2(CO_3)_{3\ (aq)}$ species newly formed in the initially Ca-free U(VI)-containing solution shows no subsequent interaction when brought in contact with bentonite.

- Realization of the conditions favoring the formation of the $Ca_2UO_2(CO_3)_{3\ (aq)}$ species at the disposal site (circumneutral pH, availability of Ca, positive or slightly negative redox potential) can be considered the worst-case disposal scenario concerning the fulfillment of the protective function of a deep geological repository with respect to uranium.

- Na-bentonite should be preferred instead of Ca-bentonite in the case of bentonite application as a retention barrier in a deep geological repository.

6 References

Amayri, S.: Synthese, Charakterisierung und Löslichkeit von Erdalkaliuranylcarbonaten M_2 $[UO_2(CO_3)_3]$ xH2O; M: Mg, Ca, Sr, Ba. *Dissertation*. FZR-359 Forschungszentrum Rossendorf, (2002).

Bernhard, G., Geipel, G., Reich, T., Brendler, V., Amayri, S., Nitsche, H.: Uranyl (VI) carbonate complex formation: Validation of the $Ca_2UO_2(CO_3)_3$ (aq.) species. *Radiochim. Acta* **89**, 511–518 (2001).

Bostick, B.C., Fendorf, S., Barnett, M.O., Jardine, P.M., Brooks, S.C.: Uranyl surface complexes formed on subsurface media from DOE facilities. *Soil Sci. Soc. Am. J*. **66**, 99–108 (2002).

Brendler, V., Geipel, G., Bernhard, G., Nitsche, H.: Complexation in the system UO_2^{2+} / PO_4^{3-} / OH^- (aq): Potentiometric and spectroscopic investigations at very low ionic strength. *Radiochim. Acta* **74**, 75–80 (1996).

Brooks, S.C., Fredrickson, J.K., Carroll, S.L., Kennedy, D.W., Zachara, J.M., Plymale, A.E., Kelly, S.D., Kemner, K.M., Fendorf, S.: Inhibition of bacterial U(VI) reduction by calcium. *Environ. Sci. Technol* **37**, 1850–1858 (2003).

Catalano, J.G., Brown Jr., G.E.: Uranyl adsorption onto montmorillonite: Evaluation of binding sites and carbonate complexation. *Geochim. Cosmochim. Acta*, **69**, 2995- 3005 (2005).

Chisholm-Brause, C.J., Berg, J.M., Little, K.M., Matzner, R.A., Morris, D.E.: Uranyl sorption by smectites: spectroscopic assessment of thermodynamic modeling. *Journal of Colloid and Interface Science* **277**, 366-382 (2004).

Geipel, G., Brachmann, T., Brendler, V., Bernhard, G., Nitsche, H.: Uranium (VI) sulfate complexation studied by time-resolved laser-induced fluorescence spectroscopy (TRLFS). *Radiochim. Acta* **75**, 199–204 (1996).

Guillaumont, R., Fanghänel, T., Fuger, J., Grenthe, I., Neck, V., Palmer, D.A., Rand, M.H.: *Chemical Thermodynamics Series Volume 5 (2003):* Update on the Chemical Thermodynamics of Uranium, Neptunium, Plutonium, Americium and Technetium. NEA OECD, Elsevier. (2003).

Jiang, J., Rao, L., Di Bernardo, P., Zanonato, P., Bismondo, A.: Complexation of uranium(VI) with acetate at variable temperatures. *J. Chem. Soc., Dalton Trans*., 1832–1838 (2002).

Karbowiak, M., Fourest, B., Hubert, S., Moulin, C.: Complexation of U(VI) with iodate ions: determination of stability constants by using spectroscopic methods and capillary zone electrophoresis. *Radiochim. Acta* **91**, 505–512 (2003).

Kato, Y., Kimura, T., Yoshida, Z., Nitani, N.: Carbonate complexation of neptunyl(VI) ion. *Radiochim. Acta* **82**, 63–68 (1998).

Kowal-Fouchard, A., Drot, R., Simoni, E., Ehrhardt, J.J.: Use of spectroscopic techniques for uranium(VI)/montmorillonite interaction modeling. *Environ. Sci. Technol*. **38**, 1399–1407 (2004).

Lopez, M., Birch, D.J.S.: Uranyl photophysics on colloidal silica: An alternative luminescence-enhancing medium for uranyl assay. *Analyst*, **121**, 905-908 (1996).

Meinrath, G.: Direct spectroscopic speciation of schoepite-aqueous phase equilibria *Journal of Radioanalytical and Nuclear Chemistry*. **232** (1-2), 179-188 (1998).

Metz, V., Amram, K., Ganor, J.: Stoichiometry of smectite dissolution reaction. *Geochim. Cosmochim. Acta*, **69**, 1755-1772 (2005).

Pashalidis, I., Czerwinski, K.R., Fanghänel, T., Kim, J.I.: Solid-liquid phase equilibria of Pu(VI) and U(VI) in aqueous carbonate systems. Determination of stability constants. *Radiochim. Acta* **76**, 55–62 (1997).

Rao, L., Garnov, A.Y., Jiang, J., Di Bernardo, P., Zanonato, P., Bismondo, A.: Complexation of uranium(VI) and samarium(III) with oxydiacetic acid: Temperature effect and coordination modes. *Inorg. Chem.* **42**, 3685–3692 (2003).

Rao, L., Zhang, Z., Zanonato, P., Di Bernardo, P., Bismondo, A., Clark, S.B.: Complexation of thorium(IV) with acetate at variable temperatures. *Dalton Trans.*, 2867–2872 (2004).

Skagius, K., Neretnieks, I.: Porosities and diffusivities of some nonsorbing species in crystalline rocks. *Water Res. Res.* **22**, 389-398 (1986).

Zanonato, P., Di Bernardo, P., Bismondo, A., Rao, L., Choppin, G.R.: Thermodynamic studies of the complexation between neodymium and acetate at elevated temperatures. *J. Solution Chem.* **30**, 1–18 (2001).

Zhang, Z., Tokunaga, T., Wan, J. : Influence of calcium carbonate on U(VI) sorption to soils. *Environ. Sci. Technol.* **37**, 5603–5608 (2003).